Chemosphere 279 (2021) 130588

Contents lists available at ScienceDirect

Chemosphere

journal homepage: www.elsevier.com/locate/chemosphere

Bioaccumulation of mercury and transcriptional responses in tusk (*Brosme brosme*), a deep-water fish from a Norwegian fjord

Pål A. Olsvik [a, b, *], Atabak M. Azad [b], Fekadu Yadetie [c]

[a] Faculty of Biosciences and Aquaculture, Nord University, Bodø, Norway
[b] Institute of Marine Research, Nordnes, Bergen, Norway
[c] Department of Biological Sciences, University of Bergen, Bergen, Norway

HIGHLIGHTS

- High levels of Hg in deep-water fish in inner parts of fjords.
- The MeHg/total Hg ratio drops in liver of tusk with high Hg levels.
- Many DEGs were differentially expressed in liver of tusk with high Hg levels.
- Top affected pathway was protein folding.
- Adipogenesis, notch signaling, and lipid metabolism pathways also affected.

ARTICLE INFO

Article history:
Received 21 February 2021
Received in revised form
8 April 2021
Accepted 12 April 2021
Available online 16 April 2021

Handling Editor: James Lazorchak

Keywords:
Deep-water fish
Mercury contamination
Transcriptional effects in liver
RNA-seq

ABSTRACT

High concentrations of mercury (Hg) have been documented in deep-water fish species from some Norwegian fjords. In this study, tusk (*Brosme brosme*) was sampled from four locations in the innermost parts of Sognefjorden in Western Norway. Total Hg and methylmercury (MeHg) levels were measured in liver tissue. To search for potential sublethal effects of Hg, we characterized the hepatic transcriptome in tusk with high and low levels of Hg bioaccumulation using global transcriptomics analysis (RNA-seq). The results showed that there was a significant correlation between fish weight and accumulated concentrations of MeHg but not total Hg. MeHg accounted for 30–40% of total Hg in liver of most of the fish, although at concentrations above 2–3 mg Hg/kg wet weight the percentage of MeHg dropped considerably. Transcriptome analysis resulted in hundreds of differentially expressed genes in the liver of tusk with high Hg levels. Functional enrichment analysis suggested that the top affected pathways are associated with protein folding, adipogenesis, notch signaling, and lipid metabolism (beta-oxidation and phospholipids). Based on transcriptional responses pointing to well-known effects of Hg compounds in fish, the study suggests that tusk in Sognefjorden could be negatively impacted by Hg bioaccumulation.

1. Introduction

Mercury (Hg) is a globally distributed pollutant of great concern. Human activities such as mining and fossil fuel combustion have significantly increased the concentration of Hg worldwide (Lamborg et al., 2014). In the marine environment Hg primarily exists as inorganic Hg, but certain bacteria can transform inorganic Hg into methylmercury (MeHg). MeHg, which is more toxic than inorganic Hg, is bioaccumulative and biomagnifies in the aquatic food web (Wiener et al., 2003). Seafood such as fish is consequently the main dietary source of MeHg exposure for humans. Many studies have documented a direct correlation between fish consumption and body burden of MeHg (Morel et al., 1998; Chapman and Chan, 2000; Cole et al., 2004; Bjornberg et al., 2005; Diez, 2009). It is therefore of interest to study bioaccumulation and mechanistic impacts of Hg in wild fish.

Recent studies have documented that deep-sea predatory fish tend to accumulate higher levels of Hg than fish living in shallower waters (Blum et al., 2013). In the North Atlantic Ocean, it has been shown that deep-dwelling fish species such as tusk (*Brosme brosme*), ling (*Molva molva*) and Greenland halibut (*Reinhardtius*

* Corresponding author. Faculty of Biosciences and Aquaculture, Nord University, Bodø, Norway.
E-mail address: pal.a.olsvik@nord.no (P.A. Olsvik).

https://doi.org/10.1016/j.chemosphere.2021.130588

hippoglossoides) may get very old and contain especially high levels of Hg (Azad et al., 2019a; Julshamn et al., 2011; Maage et al., 2012; Kvangarsnes et al., 2012). Furthermore, deep-sea fish inhabiting Norwegian fjords have been shown to contain high levels of Hg (Olsvik et al., 2013; Azad et al., 2019b). For example, tusk and Atlantic cod (*Gadus morhua*) caught in the open-sea Lofoten area in Northern Norway accumulated less Hg than their cousins living in fjords (Maage et al., 2012; Azad et al., 2019a, 2020). The high levels of Hg in deep-sea fish in fjords in Norway has raised concerns about seafood safety, because they can bioaccumulate Hg to levels exceeding the maximum legal limits allowed for human consumption.

Several explanations have been launched to explain why long-lived deep-sea predatory fish tend to bioaccumulate high levels of Hg. In the Pacific Ocean it has been shown that sunlight degrades up to 80% of MeHg in surface waters, while below 50 m most of the MeHg remains in the food web (Blum et al., 2013). Top predators in food webs in shallower water will thus accumulate less MeHg than fish inhabiting deeper zones. In fjords, physical properties such as water residence time (exchange of fjord water above the sill), density stratification, and intertidal waves may contribute to higher MeHg levels in deep-water organisms. It has been shown that fjord water at 15 m depth is exchanged more often than water at 50 m depth (Asplin et al., 2014). In addition to atmospheric Hg deposition, fjord ecosystems are also affected by industrial point-sources and terrestrial runoff (Azad et al., 2019a). MeHg produced by bacteria below the surface mixed layer contributes heavily to uptake into the marine food web (Blum et al., 2013), a phenomenon especially favored in fjord ecosystems.

MeHg is the dominant form of Hg in fish. Fish muscle typically contains 80–100% MeHg while liver may contain considerably less MeHg compared to inorganic Hg (Grieb et al., 1990; Bloom, 1992; Maage et al., 2012; Batchelar et al., 2013; Olsvik et al., 2013). MeHg is a potent neurotoxicant that might damage the central nervous system in organisms. Exposure to MeHg might cause a variety of disorders in fish, including reduced growth, endocrine disruption, reduced spawning success, immunosuppression and damage to organs such as liver and kidney (Klaper et al., 2008). Cytotoxicity of MeHg has been linked to disruption of intracellular Ca^{2+} homeostasis, and disruption of proteins containing cysteine and methionine (Ceccatelli et al., 2010). Due to its ability to bind to thiol (SH) or selenol (SeH) groups present in biological molecules, MeHg can cause disruption of enzymatic function (Ceccatelli et al., 2010; Farina et al., 2011a). At the molecular level, pathways often reported disrupted by MeHg exposure in fish include energy metabolism, oxidative stress, apoptosis, immune response, and lipid metabolism (Gonzalez et al., 2005; Berg et al., 2010; Cambier et al., 2010; Richter et al., 2011; Olsvik et al., 2011, 2013; Yadetie et al., 2013, 2016).

This study aimed to examine differential gene expression in liver of a deep-sea predatory fish species from a Norwegian fjord with high Hg concentration. Using longline fishing, 35 tusk were caught in Sognefjorden, situated in Western Norway, in the summer of 2015. As a follow-up of our previous field (Olsvik et al., 2013; Azad et al., 2019a, 2019b, 2020) and laboratory studies (Olsvik et al., 2011, 2015; Yadetie et al., 2013, 2016) with Hg in fish, this study was designed to look for molecular targets and mechanisms of effects of Hg exposure in liver of fish with varying levels of bioaccumulated Hg. Earlier studies have shown that there is a gradient of Hg in fish from fjords from Western Norway, with higher Hg concentration in fish caught in the innermost parts (Olsvik et al., 2013; Azad et al., 2019b, 2020). By comparing transcriptomics profiles in fish with low and high levels of Hg using RNA-seq, we explore molecular targets and identify potential biomarkers of environmental Hg exposure in tusk collected from a contaminated fjord.

2. Materials and methods

2.1. Study area

Sognefjorden is Norway's longest and deepest fjord stretching 205 km inland from the ocean and reaching a maximum depth of 1308 m and a middle depth of more than 1000 m. It is located at 61°N in the Northeast Atlantic Ocean in Western Norway (Fig. 1). In most parts, a U-shaped profile in cross-section reflects that the fjord was once carved out by an arm of a glacier. A sill at the mouth of the fjord at about 300 m depth limits the free flow of water between the fjord and open ocean. The fjord branches out into several side arms in the inner parts and is considered a highly complex ecosystem with dynamic water residence times and circulation patterns. Even though no local point sources of Hg are known, deep-water fish from Sognefjorden contains elevated levels of Hg (Azad et al., 2020), resulting in a dietary warning issued by the Norwegian Food Safety Authority against human consumption of certain fish species from this fjord.

2.2. Animal sampling

Using longline fishing, 35 tusk were caught from four locations in the innermost parts of Sognefjorden in May–June 2015. Tusk were sampled from four locations including Site 1, Lusterfjord (250–500 m depth); Site 2, Årdalsfjord (350–450 m depth); site 3 (300–400 m depth) and site 7, main sector of fjord (300–1000 m depth). More details about the sampling sites are given by Azad et al. (2020). After sampling, weight and length were measured, and otoliths collected for age determination. Liver samples were frozen at −20 °C for chemical analysis and preserved in RNAlater (Thermo-Fisher Scientific) for RNA extraction. For chemical analysis, liver samples were homogenized first and analyzed without lyophilization due to the high fat content.

2.3. Metal analysis

Total Hg, cadmium (Cd), arsenic (As) and selenium (Se) concentrations were quantified with inductively coupled plasma-mass spectrometry (ICP-MS) following microwave digestion as previously described by Julshamn et al. (2011). The accuracy and precision of the method have been tested by analyzing certified reference materials (CRM's) including CRM1566 (oyster tissue) from the National Institute of Standards and Technology (Gaithersburg, USA) and TORT-3 (lobster hepatopancreas) from the National Research Council (Ottawa, Canada) in each run and the recoveries of Hg ranged from 80% to 120%. The limits of quantification (LOQ) of this method were 0.005 mg kg-1 dry weight (dw) for Hg and Cd and 0.01 mg kg-1 dw for Se and As. MeHg in liver was quantified with isotope dilution GC-ICP-MS using an Agilent 6890 N gas chromatograph coupled to an Agilent 7500a ICP-MS instrument. The extraction procedure and the details on the GC-ICP-MS method are described elsewhere (Valdersnes et al., 2012). LOQ for MeHg was 0.003 mg kg-1 dw, and the measurement uncertainty was 20% at concentration >0.2 mg/kg.

2.4. Organic persistent pollutants

A majority of the studied tusk were analyzed for a wide range of persistent organic pollutants as part of a seafood safety surveillance program. Data were obtained from liver of all low Hg tusk ($n = 8$) and 16 out of 28 of the high Hg tusk. Dioxins and dioxin-like PCBs and PCBs were quantified with certified methods as previously described by Lundebye et al. (2017). Briefly, dioxins (PCDDs (include 2,3,7,8-TCDD, 1,2,3,7,8-PeCDD, 1,2,3,4,7,8-HxCDD,

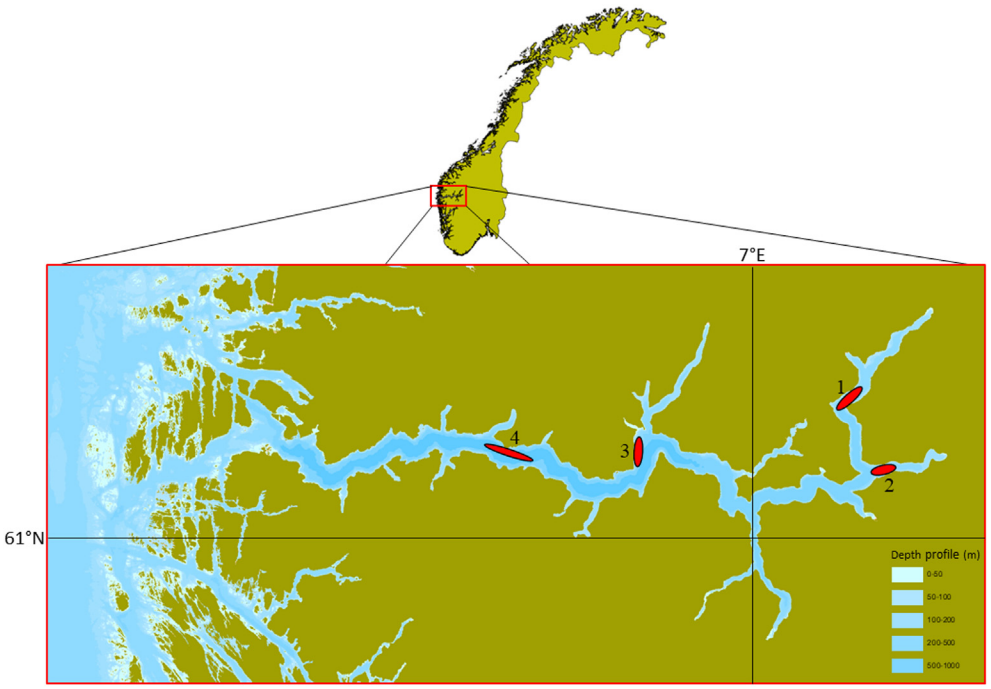

Fig. 1. Tusk sampling sites (red areas) from 2015 from Sognefjorden, Norway. (For interpretation of the references to color in this figure legend, the reader is referred to the Web version of this article.)

1,2,3,6,7,8-HxCDD, 1,2,3,7,8,9-HxCDD, 1,2,3,4,6,7,8-HpCDD and OCDD) and PCDFs (include 2,3,7,8-TCDF, 1,2,3,7,8-PeCDF, 2,3,4,7,8-PeCDF, 1,2,3,4,7,8-HxCDF, 1,2,3,6,7,8-HxCDF, 1,2,3,7,8,9-HxCDF, 2,3,4,6,7,8-HxCDF, 1,2,3,4,6,7,8-HpCDF, 1,2,3,4,7,8,9-HpCDF and OCDF)) and non-ortho-PCBs were analyzed by high-resolution gas chromatography/high resolution-mass spectrometry (HRGC-HRMS). Mono-ortho-PCBs were analyzed by gas chromatography/tandem mass spectrometry (GC–MS/MS). Concentrations of these compounds were converted into toxic equivalents (TEQ), ng TEQ/kg wet weight using WHO2005s TEF approach (Van den Berg et al., 2006). Sum PCB7 includes some of the most common non-dioxin like PCB congeners found in nature (PCB 28, 52, 101, 118, 138, 153 and 180) (EFSA, 2005). The sum PBDE7 congeners 28, 47, 99, 100, 153, 154, 183 were analyzed by GC-MS NCI (negative chemical ionizing) as described by Julshamn et al. (2013).

2.5. RNA isolation

Liver tissue from each of 35 individual tusk was thoroughly homogenized for RNA extraction using a Precellys 24 homogenizer (Bertin Technologies, Montigny-le-Bretonneux, France). Total RNA from fish liver was extracted using the RNeasy Plus mini kit (Qiagen, Germany) according to the manufacturer's instructions. RNA quality was evaluated with the NanoDrop ND-1000 UV–Vis Spectrophotometer (NanoDrop Technologies, USA) and the Agilent 2100 Bioanalyzer (Agilent Technologies, USA). The RNA integrity number (RIN) was 8.5 ± 0.5 in liver of tusk (mean ± SEM).

2.6. RNA sequencing and quantification

RNA-seq was used to explore transcriptome changes and screen for potential biomarker of Hg exposure in each of the 35 individual tusk liver sample. Briefly, 1.5 μg RNA per sample was used as input material for the RNA-seq sample preparations. Sequencing libraries were generated using NEBNext UltraTM RNA Library Prep Kit for Illumina® (NEB, USA). Library preparations were sequenced on an Illumina HiSeq 4000 platform and 150-base-pair paired-end reads were generated. About 50 million paired-end raw reads were obtained for each sample. All downstream analyses were based on clean data with high quality after removing adapters, ploy-N and low-quality reads. Sequencing, *de novo* transcriptome assembly using Trinity (Grabherr et al., 2011), read mapping using TopHat2 and quantification by RSEM (Li et al., 2012) were performed by Novogene (Cambridge, UK). The quantified raw read counts of Unigene clusters for the individual samples were processed in-house in differential expression and downstream analysis.

2.7. Differential expression and pathway analysis

Differential expression analysis of RNA-seq data was performed with edgeR, using the Biocoductor RnaSeqGeneEdgeRQL package (Chen et al., 2016). All zero and low counts (normalized count < 1) were removed, leaving about 70,000 Unigene clusters. Out of the Unigene clusters which include redundant genes, 17400 putative unique genes were mapped to orthologs in the Atlantic cod (*Gadus morhua*) genome (Ensembl.org) by reciprocal blast. The Atlantic cod is a gadoid fish species related to tusk with a well-studied genome. This was done to facilitate downstream functional analysis. Using an FDR <0.05 and fold-change of at least 1.5 cutoff resulted in 1230 differentially expressed genes (DEGs) (Supplementary file 2). Differential expression analysis using edgeR was based on comparison of high Hg ($n = 28$) and low Hg ($n = 7$) groups (Table S1, Supplementary file 1).

The pathway analysis was performed using the human orthologs of the Atlantic cod DEGs, retrieved using the Ensembl Biomart tool (Ensembl.org). The DEGs were mapped to human orthologs and used for pathway enrichment analysis with tools such as Enrichr (Kuleshov et al., 2016), STRING protein-protein interaction (String.org), MetaCore (Thompson Reuters, Genego, St. Joseph, MI, USA), and Ingenuity Pathway Analysis (IPA) (Qiagen, Redwood City, CA, USA). Hierarchical clustering analysis (Euclidian metric, complete linkage) was performed in Qlucore Omics Explorer 3.4

(Qlucore AB, Lund, Sweden), using log2-transformed library size-normalized cpm (counts per million reads) values. Genes differentially expressed in multi group comparison (Qlucore Omics Explorer, q-value < 0.05) were used for hierarchical clustering. Causal network and upstream regulator analyses were performed in IPA (Kramer et al., 2014). Upstream regulator analysis determines likely molecules or chemicals that are connected to dataset genes through a set of direct or indirect relationships. Predicted activation or inhibition are calculated by using the direction of gene regulation (up or down-regulation).

2.8. Statistics

One-way ANOVA with Tukey's post hoc test was used to compare weight, Hg, MeHg and Se concentration between the fishing locations. In case the SDs differed significantly (Brown-Forsythe test), or the data did not have a normal distribution (Shapiro-Wilk test), the data were log-transformed before ANOVA. For hierarchical clustering of RNA-seq data, log2-transformed expression values (normalized RNA-seq cpm) were analyzed in Qlucore Omics Explorer (Qlucore, Lund, Sweden), using multi-group comparison test (ANOVA) with Benjamini-Hochberg false discovery rate (FDR) correction for multiple hypotheses testing, to identify top discriminating genes.

3. Results

3.1. Wild-caught fish

An overview of fish size and sex is presented in Table 1. There were no significant differences in weight or length between tusk caught at the four locations. On average, fish weight and length were 3.31 ± 0.26 kg and 66.1 ± 1.65 cm, respectively (n = 35, mean ± SEM). At the two innermost locations, mainly males were caught, whereas a more balanced sex ratio was obtained for the two outermost locations in the main fjord.

3.2. Hg and MeHg in liver

Mean total Hg in liver of tusk varied from 2.18 ± 0.39 mg/kg at the innermost location (n = 8) of the fjord to 0.83 ± 0.06 mg/kg at location 3 (n = 8, mean ± SEM, Table 1). Further out in the fjord, at location 4, there was a large individual variation in the accumulated levels of total Hg. Four individuals caught at location 4 contained very high levels of total Hg in the liver (n = 4, 7.97 ± 2.82 mg/kg), and these fish were distinctly different than the other eight fish caught at this location in terms of Hg accumulation (0.27 ± 0.05 mg/kg, n = 8). By omitting the four individuals from location 4 with very high concentrations of total Hg, the general pattern of Hg accumulation was from high levels in the innermost parts to lower levels further out in the fjord (Table 1). Tusk from location 3 and 4 (without the four deviating individuals) contained significantly lower concentrations of total Hg than tusk from location 1 (t-test, $p < 0.0001$). The same pattern was seen for MeHg, with tusk from locations 3 and 4 (without the four deviating individuals) containing significantly lower concentrations of MeHg in liver compared to location 1 (t-test, $p < 0.0001$).

Accumulated levels of MeHg (p = 0.03), but not total Hg (p = 0.26), was significantly correlated with fish weight (Fig. 2A). MeHg levels in liver were strongly correlated with total Hg (Spearmen's rank correlation, r = 0.80, $p < 0.0001$). On average, MeHg accounted for 36% of total Hg in liver of the studied tusk (n = 35). MeHg accounted for 30.3% of total Hg in liver from tusk from location 1, 27.7% at location 2, 43.4% at location 3 and 51.9% at location 4 (minus the four deviating individuals). In liver of the four deviating individuals from location 4, MeHg accounted only for 9.5% of total Hg (Table 1). The data shows that when the accumulated concentration of total Hg in the liver of the studied tusk is above 2–3 mg/kg, the MeHg to total Hg ratio drops quickly (Fig. 2B). The age of the studied tusk, as determined by structural pattern of otolith growth rings (recorded for 29 out of the 35 studied tusk by the Marine and Freshwater Research Institute (MFRI), Iceland), varied between 9 and 16 years old (12.3 ± 0.3 years, mean ± SEM, n = 29). Fish age correlated significantly with both MeHg and total Hg levels in the liver (Spearman's rank correlation, MeHg, p = 0.002, total Hg, p = 0.006).

Because of these four deviating individuals from location 4, we decided to separate the fish based on accumulated levels of total Hg independent of the location they were caught in the downstream transcriptional analyses. To explore possible Hg-level dependent changes in gene expression using Qlucore OMICs Explorer, the samples were first grouped based on Hg levels (irrespective of sampling site) into Hg-group 1 (0–0.49 mg/kg), Hg-group 2 (0.50–0.99 mg/kg), Hg-group 3 (1.0–1.99 mg/kg) and Hg-group 4 (above 2.0 mg/kg), with average Hg levels of 0.23, 0.76, 1.52 and 5.30 mg/kg, respectively (Supplementary file 1)Table S1. Based on the exploratory hierarchical clustering and PCA analysis, the samples in Hg groups 2–4 were merged making only two categories of low and high Hg-groups, consisting of seven fish with uniformly low liver levels of Hg from the outermost fjord location (location 4) (n = 7, 0.23 ± 0.13 mg/kg) and 28 fish with high Hg levels (n = 28, 2.49 ± 3.08 mg/kg) (Table 2). These two groups were compared for differential gene expression analysis in response to high Hg levels in tusk.

Table 1
Overview of the studied tusk from Sognefjorden and various contaminant levels, including concentrations of total Hg, MeHg and organic contaminants in liver. Values are concentrations in wet weight (mean ± SEM). Letters denote statistical significance. *For organic contaminants, site 1: n = 7, site 3: n = 6, site 4: n = 8, site 4 high: n = 3.

	Site 1 - Lusterfjord	Site 2 - Årdalsfjord	Site 3 - Main fjord 1	Site 4 - Main fjord 2	Site 4 - high Hg
Catch depth (m)	250–350	350–450	250–400	300–400	700–1000
Number of fish	8	7	8	8	4
Sex ratio (m/f)	7/1	7/0	4/4	6/2	2/2
Weight (kg)	3.08 ± 0.37	3.58 ± 2.33	3.85 ± 0.82	2.71 ± 0.15	3.58 ± 2.71
Length (cm)	64.9 ± 2.8	68.7 ± 2.3	68.8 ± 5.0	63.1 ± 1.3	70.0 ± 7.7
Total Hg (mg/kg)	2.18 ± 0.39^{a}	1.91 ± 0.29^{ab}	0.83 ± 0.06^{b}	0.27 ± 0.05^{c}	7.97 ± 2.82^{d}
MeHg (mg/kg)	0.66 ± 0.08^{a}	0.53 ± 0.08^{a}	0.36 ± 0.07^{bc}	0.14 ± 0.04^{c}	0.76 ± 0.14^{a}
Percent MeHg	30.3%	27.7%	43.4%	51.9%	9.5%
Se (mg/kg)	5.76 ± 0.74^{ab}	5.43 ± 0.50^{ab}	5.10 ± 1.17^{a}	4.76 ± 0.31^{ab}	9.86 ± 2.71^{b}
Cd (mg/kg)	0.21 ± 0.05^{a}	0.17 ± 0.03^{ab}	0.23 ± 0.08^{ab}	0.07 ± 0.01^{b}	0.64 ± 0.24^{ab}
As (mg/kg)	14.75 ± 2.83^{ab}	17.24 ± 3.62^{a}	7.60 ± 0.76^{b}	8.86 ± 1.10^{ab}	8.60 ± 1.27^{ab}
Sum dioxins and DL-PCBs (pg/g (TEQ), UB LOQ)*	29.60 ± 4.95		34.83 ± 2.34	28.63 ± 3.35	39.39 ± 4.48
Sum PCB_7 (28, 52, 101, 118, 138, 153, 180) (ng/g UB LOQ)*	1929 ± 235.8^{a}		1330 ± 294.6^{ab}	409.3 ± 76.16^{b}	2396 ± 2233^{ab}
Sum $PBDE_7$ (28, 47, 99, 100, 153, 154, 183) (ng/g)*	160.0 ± 20.12^{a}		111.0 ± 29.82^{ab}	32.88 ± 7.78^{b}	131.3 ± 119.5^{ab}

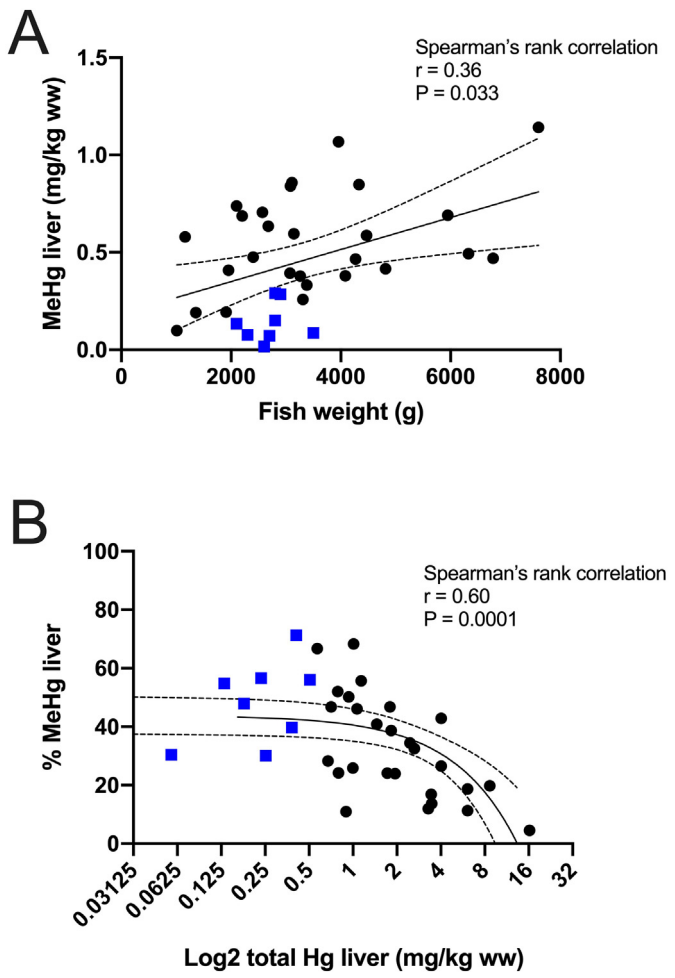

Fig. 2. Correlation between A) fish weight (g) and MeHg (mg/kg wet weight) and B) total Hg (mg/kg wet weight) and MeHg (%) in liver of tusk from four locations in Sognefjorden, Norway. The figures show linear regression with 95% confidence intervals. ■ = low Hg group, ● = high Hg group used in transcriptional comparison. N = 35.

significantly for dioxins and dioxin-like PCBs. After separating the tusk based on accumulated concentrations into a high and low Hg group, liver in tusk from the high-Hg group contained significantly higher concentrations of dioxins and dioxin-like PCBs and PCBs than liver from the low-Hg tusk (Table 2). Differences were 3.9 higher for PCBs and 1.7-times higher for the dioxins and dioxin-like PCBs.

Of other potential confounding chemicals, Cd, As and Se were also quantified in liver of each of the 35 tusk. Of these, significantly lower Cd concentrations were observed in liver of tusk from location 4 compared to location 1 (Table 1). Cd was also higher in the high Hg group than in the low Hg group (Table 2). For As and Se, there were no differences between the high Hg group and the low Hg group (Table 2).

3.4. Sequencing output

On average, 46.8 million raw reads were sequenced from each liver sample (46.8 ± 4.4 million reads, mean ± st.dev., $n = 35$). The sequencing details are shown in Table S2 (Supplementary file 1).

3.5. Genes and pathways affected in tusk with high levels of Hg

3.5.1. Hierarchical clustering

Exploratory analysis of the RNA-seq data using hierarchical clustering and PCA (Fig. 3A and B) in Qlucore OMICs Explorer showed that the samples are separated into two groups of low Hg (Hg-groups 1) and high Hg (Hg-groups 2–4) groups, with no clear Hg-level dependent expression in the latter group (Qlucore Multi-group test, FDR < 0.05). Further exploration using Qlucore showed that sex and length of fish had little effect on differential gene expression. Based on these exploratory analyses, differential gene expression analysis was performed between low Hg and high Hg groups. The top 323 genes differentially expressed discriminating between the two groups using Qlucore two-group test (FDR < 0.05) are shown in Table S3 (Supplementary file 1). Most of these genes (about two-third) are subset of the larger group of DEGs identified using edgeR (Supplementary file 2). Similarly, many of the pathways enriched in the 323 top genes shown in the string network (Fig. 4, Supplementary file 5) are also enriched in the larger set of DEGs

Table 2
Concentrations of Hg, MeHg and Cd, as well as organic pollutants in liver of tusk from Sognefjorden after separation of the fish into a low and high Hg group. Low Hg group: $n = 7$, high Hg group: $n = 28$ for Hg, MeHg, Cd, Se and As, and $n = 17$ for organic pollutants. Values are wet weight concentrations (mean ± SEM). Statistical significance of comparisons is shown in the figure (*t*-test or Mann Whitney *U* test). Asterisks show significant differences between the two groups. T-test, $p < 0.05$=*, $p < 0.01$=**, $p < 0.001$=***, $p < 0.0001$=****.

Compound	Unit	Low Hg group (n = 7)	High Hg group ($n = 28/17$)	*t*-test or Mann Whitney, *p*-value
Hg	mg/kg	0.23 ± 0.02	2.49 ± 0.58****	0.0001
MeHg	mg/kg	0.12 ± 0.02	0.54 ± 0.05****	0.0001
Cd	mg/kg	0.07 ± 0.01	0.26 ± 0.05***	0.0006
Se	mg/kg	4.64 ± 0.33	6.05 ± 0.60	0.2331
As	mg/kg	8.29 ± 1.08	12.39 ± 1.41	0.1802
Sum dioxins and DL-PCBs	pg/g (TEQ), UB LOQ	63.42 ± 6.06	110.09 ± 10.0**	0.0042
Sum PCB_7 (28, 52, 101, 118, 138, 153, 180)	ng/g UB LOQ	409.3 ± 76.2	1792 ± 395*	0.0232
Sum $PBDE_7$ (28, 47, 99, 100, 153, 154, 183)	ng/g LB LOQ	9.21 ± 2.65	39.22 ± 8.32	0.0529

3.3. Other contaminants in liver

Table 1 shows the accumulated concentrations of dioxins and dioxin-like PCBs, PCBs and PBDEs in liver of 24 out of the 35 studied tusk. Except for the four deviating individuals at location 4, there were significantly lower PCB and PBDE concentrations in liver of fish from location 4 compared to location, suggesting a fjord gradient with highest PCB and PBDE concentrations in fish from the innermost areas. The location-based concentrations did not differ (Supplementary file 2) (see 3.5.2 below). The heatmap was made from normalized log2 cpm values (edgeR) using Qlucore software (log2cpm > 5 in at least 50%, FDR < 0.05, fold-change > 1.5).

To explore possible confounding effects from organic pollutants, we performed similar differential expression analysis in high versus low Hg-groups for a subset of the dataset (24 samples for which organic pollutant levels were available) as detailed in Supplementary file 6. The analysis resulted in 239 and 194 differentially expressed genes before and after controlling for the levels of sum of

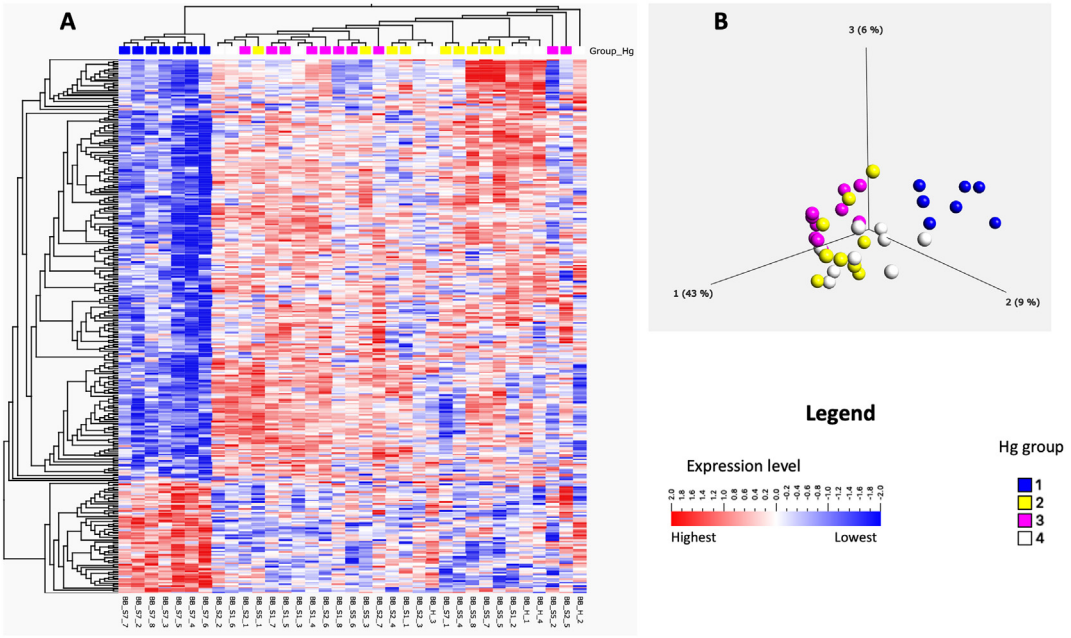

Fig. 3. Hierarchical clustering and principal component analysis (PCA) of samples with increasing Hg-levels (Hg groups 1–4) based on RNA-seq data. Clustering (A) and PCA (B) show clear separation of samples into low Hg (Hg groups 1) and high Hg (Hg groups 2–4) groups based on gene expression (Qlucore Omics Explorer, multigroup test FDR q-value < 0.05). Data represent log2 transformed expression values (normalized RNA-seq cpm) of individual tusk liver from different sampling sites. The color bar indicates gene expression levels ranging from highest at deep red end to lowest at the deep blue end. Hg-groups 1, 2, 3 and 4 have average Hg levels of 0.23, 0.76, 1.52 and 5.30 mg/kg, respectively. (For interpretation of the references to color in this figure legend, the reader is referred to the Web version of this article.)

the AHR activators (dioxins and dioxin-like PCBs), respectively (Supplementary file 6, Fig. S2A. The overlapping lists, with 133 of the 194 genes shared with the 239 list, included most of the genes that appear to be related to Hg effects such as the chaperons and the copper transporting ATPase, *aatp7b* (Supplementary file 6, Fig. S2A-C, Fig. 4, Supplementary file 5). Similar results were obtained after controlling for the levels for sum of PCB 7 (Supplementary file 6; Fig. S3A and B).

3.5.2. DEGs and pathways enriched

Analyzing differential expression with edgeR and using a cutoff of FDR<0.05 and fold-change of at least 1.5, there were 1230 DEGs in liver of wild tusk with high levels of Hg (Supplementary file 2). Of these, 852 DEGs could be annotated with unique human orthologs for pathway enrichment analysis. The most significant DEG with annotation was serum response factor (*srf*), followed by protein S (*pros1*) and bromodomain containing 7 (*brd7*). Ranked by fold change, *abcb6* (fold-change 933), *crebbp* (fold-change 571) and *nsd1* (fold-change 434) showed the biggest expression difference. According to the curated chemical-gene interactions listed for mercuric chloride and methylmercuric chloride in the Comparative Toxicogenomic Database (CTD), 35 out of 852 (4.1%) DEGs with unique identifiers were common between the tusk DEG data and mercuric chloride (ctd:D008627). 269 out of the 852 (31.6%) DEGs were common between the tusk data and methylmercuric chloride (ctd:C004925), while 37 DEGs (4.3%) were common between all three gene lists. Thus, about 40% of the significant DEGs in liver of tusk have previously been linked to toxic effects of Hg compounds, confirming Hg specific effects on the tusk genes. The comparison is shown in Fig. 5A, while the DEGs unique for the tusk data, and common with mercuric and methylmercuric chloride (and both) are shown in Table S4 (Supplementary file 1).

Table S5 (Supplementary file 1) shows the most significant Gene Ontologies (input 1230 DEGs), analyzed with the ToppGene Suite (Chen et al., 2009). Gene Ontology analysis pointed to many generic biological processes and molecular functions. In terms of known effects of Hg, a few interesting categories still stand out. For example, the dataset contained 132 DEGs associated with neurogenesis (GO:0022,008), and 32 DEGs associated with cellular response to steroid hormone stimulus (GO:0071,383). Furthermore, the gene list contained 60 DEGs associated with lipid binding (GO:0008289).

The enrichment analysis showed that cell morphogenesis involved in differentiation (GO:0000904) was the most significant ontology, followed by actin cytoskeleton organization (GO:0030,036) and small GTPase mediated signal transduction (GO:0007264). Enrichment analysis also pointed to differential expression of genes associated with lipid metabolism (Reactome pathway R-HSA-556833). Fig. 5B shows the 20 most significant pathways as analyzed with the Metascape tool (Zhou et al., 2019). Table 3 shows the most significant Wikipathways as analyzed with the Enrichr tool. Wikipathways ranked *notch signaling pathway* (WP61), *androgen receptor signaling pathway* (WP138) and *nuclear receptors* (WP170) as the pathways most affected in liver of tusk with high levels of Hg. Here, it was also interesting to see mechanisms associated with the aryl hydrocarbon receptor (AhR) ranking among the top pathways (WP2586), based on among others differential expression of *cyp1a1*. An impact on notch signaling was also suggested by Metacore analysis (Supplementary file 3). Fig. 6 shows the *stem cells NOTCH in inhibition of WNT/Beta-catenin-induced osteogenesis* pathway with significant DEGs and interactions highlighted (the top Metacore pathway map), and how the pathway affects adipocyte differentiation.

Protein folding was among the significant process networks, according to Metacore analysis, based on differential expression of genes encoding HSP90, P300, HSP70, HSPA2, HSP40, Calcineurin A (alpha) (*ppp3ca*), TCP1-beta (*cct2*), DNAJB6 (Hdj-1), HSP10 (mitochondrial), TCP1-delta (*cct4*), Endoplasmin (*hsp90b1*), BAG-3, Calcineurin A (catalytic), CDC37, TCP1-epsilon (*cct5*) (Fig. 7). Fig. 4 also shows a STRING interaction network and enriched processes

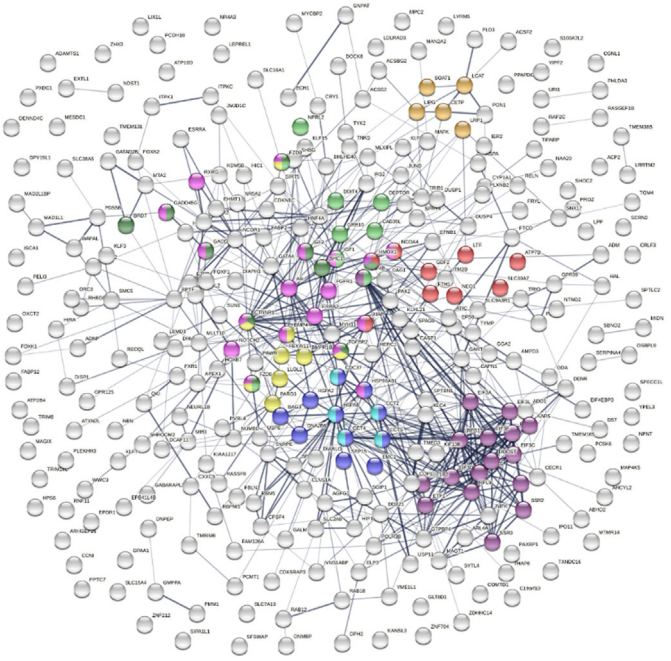

GO- term/pathway	description	FDR
GO:0055076	transition metal ion homeostasis	0.0059
GO:0006457	protein folding	0.0159
HSA-72766	Translation	0.0028
hsa04979	Cholesterol metabolism	0.0327
hsa05225	Hepatocellular carcinoma	0.0322
hsa04150	mTOR signaling pathway	0.0327
hsa04390	Hippo signaling pathway	0.0327
hsa05200	Pathways in cancer	0.0377
GO:0101031	chaperone complex	0.0013

Fig. 4. STRING protein-protein interaction network of the top discriminating 323 genes (Table S2) between low and high Hg groups (Qlucore two-group test, FDR q-value < 0.05). In the lower panel, some of the significantly enriched pathways are shown with color legend corresponding to the nodes in the network. The whole list of enriched pathways is shown in Supplementary file 5. (For interpretation of the references to color in this figure legend, the reader is referred to the Web version of this article.)

protein folding and *chaperone complex*. The Metalcore process network, *protein folding - Folding in normal condition* pathway is shown in Fig. 7. The enriched pathways using the different tools suggest that DEGs encoding proteins involved in protein stability and folding were differentially expressed.

Exposure to Hg can lead to increased incidents of misfolded proteins in cells due to oxidative stress. Interestingly, pathways associated with oxidative stress were not among the most significantly affected in this dataset. Nevertheless, eight genes in the GO term response to oxidative stress (GO:0006979), *hmox1*, *bmp4*, *rbpms*, *gab1*, *adar*, *pxn*, *mbl2* and *gpx4*, were differentially expressed. Several other genes belonging to oxidative stress-related GO terms were also differentially expressed, i.e. cellular response to oxidative stress (GO:0034,599): *kat2b*, *atf4*, *mgmt*, negative regulation of oxidative stress-induced neuron death (GO:1903204): *nr4a3*, *atf4*, *ncoa7* and *ctnnb1*, and negative regulation of oxidative stress-induced cell death (GO:1903202): *gata4*. Three genes associated with biosynthesis, metabolism and transport of glutathione, *chac1*, *gpx4* and *gja1*, were differentially expressed. Furthermore, seven genes linked to *oxidative stress induced senescence* (REACT:R-HSA-2559580), *rbbp7*, *mdm4*, *tnrc6b*, *cbx8*, *kdm6b*, *tnik* and *map4k4*, were differentially expressed.

Metacore metabolic network analysis furthermore pointed to Hg-induced effects on pathways linked to lipid metabolism. Figure S1 (Supplementary file 1) shows the phosphatidylcholine and acyl-L-carnitine pathways, of particular interest in terms of Hg-induced effects in fish. Impact on these two pathways points to Hg interactions with phospholipid membranes and possible effect on overall energy metabolism. Alternatively, it could be due to interference with enzymatic activities by binding sensitive SH groups of enzymes and inactivating them. Causal network analysis predicted TGFB1, TP53, tretinoin and RXFP2 as possible top upstream regulators with predicted activated state (z-score above 2), while actinomycin D was predicted as the most significantly inhibited regulator with a z-score less than −2. Upstream regulators are shown in Supplementary file 4.

4. Discussion

4.1. Mercury in Sognefjorden

This study shows that the accumulated levels of Hg in liver of tusk inhabiting the innermost parts of Sognefjorden varies a lot, with concentrations ranging from 0.06 to 16.21 mg Hg/kg wet weight in the studied fish. The latter value is very high in terms of what is normally found in liver of tusk from the North Atlantic (Rua-Ibarz et al., 2019), and well above the maximum legal limit for most fish species (0.5 mg Hg/kg) (EU, 2006). We have found even higher Hg concentrations in tusk from Hardangerfjorden, further south in Norway, with average liver levels at 6.39 mg/kg wet weight (Azad et al., 2019b). Very high degree of Hg accumulation in deep-sea fish from fjords may rely on several factors. Fjords typically receive runoff from large catchment areas, and in fjords with shallow sills (like Sognefjorden) water exchange can be restricted. This runoff may wash the atmospherically deposited Hg species as well as MeHg produced in the catchment. The main rivers with large catchments empty in the inner part of the Sognefjord and therefore the inner part receives higher amounts of terrestrial Hg species. A clear gradient in the stable carbon isotope has been documented in tusk from Sognefjorden. A gradual shift in the source of carbon in the base of the food web indicating inclusion of more terrestrial carbon in the base of food web in the inner part of Sognefjord has been suggested as a reason for this trend (Azad et al., 2021). This means that both long-range atmospheric transport and local point-sources may contribute to the high levels of Hg in fjords in Western Norway. Fjords can also have stratification layers due to temperature and salinity differences which may impact the degree of microbial methylation of Hg. Microbial methylation of inorganic Hg is commonly observed in low-oxygen coastal sediments (Blum et al., 2013). Microbial methylation of inorganic Hg may also happen in the water column (Wang et al., 2018).

Excluding 4 individuals, there was a distinct gradient of decreasing levels of accumulated Hg in the fish outward in the fjord. However, the four deviating individuals with highest Hg concentrations were all from location 4, the outermost mid-fjord site. The hook depth where these four individuals were caught was down to 1000 m, the deepest fishing ground explored in the present study. It is therefore possible that Hg bioaccumulation in tusk increases with water depth. Interestingly, the ratio of MeHg to total Hg were lowest in individuals with highest Hg levels. In fish muscle, Hg is mainly present in organic form. In fish liver, however, the MeHg/total Hg ratio can be lower. In a previous study of tusk from Hardangerfjorden, we observed that MeHg only accounted for 11–30% (mean 17%) of total Hg in the liver (Olsvik et al., 2013). In this study, MeHg ranged from 5 to 71%, with a mean level of 36 ± 3% (mean ± SEM, n = 35). Whether this variation reflects direct dietary

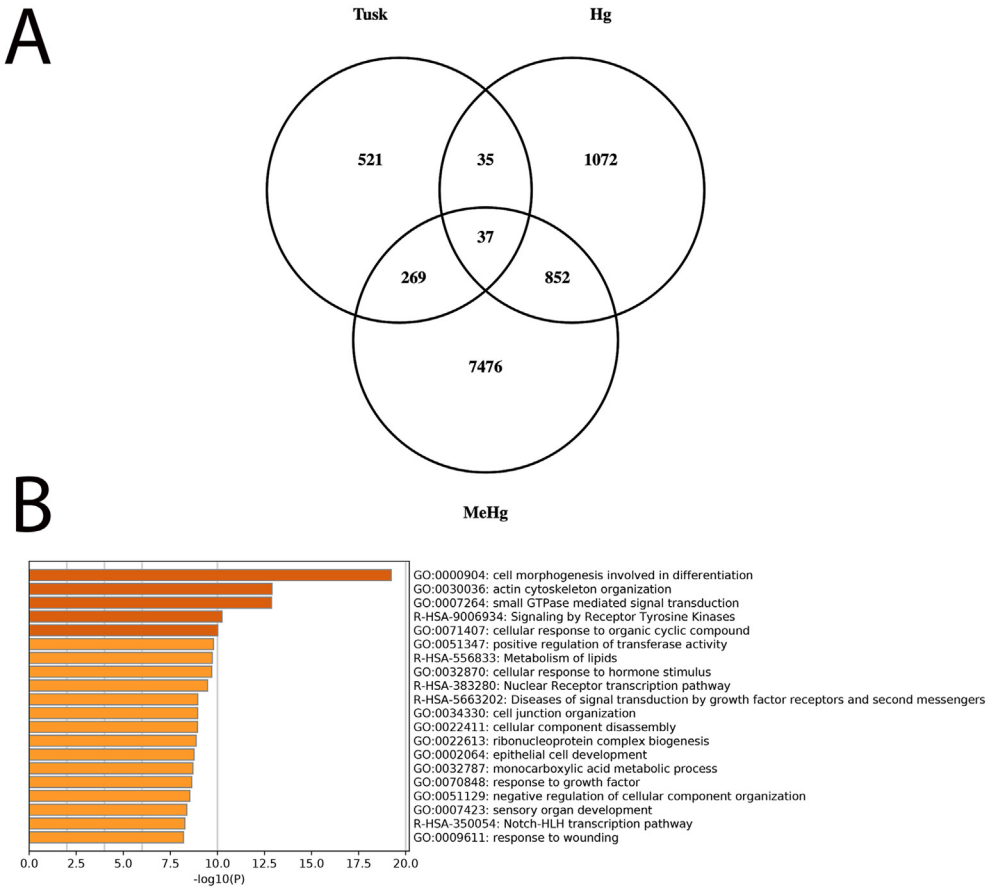

Fig. 5. A) Venn diagram showing overlap with edgeR DEG gene list and curated chemical-gene interactions in the CTD. Input in the figure were 852 DEGs in tusk liver, 1996 genes with interactions with mercuric chloride (ctd:D008627), and 8634 genes with interactions with methylmercuric chloride (ctd:C004925). B) Metascape enrichment analysis of DEGs in high Hg group. Top 20 significantly enriched (q-value < 0.05) clusters of pathways and processes with their representative enriched terms.

uptake of inorganic Hg from bottom-dwelling organisms, or demethylation mechanisms and accumulation of inorganic Hg in the liver is not known. While MeHg is absorbed readily by the gastrointestinal tract of animals (Bridges and Zalups, 2017), it has been shown that less than 10% of dietary inorganic Hg is absorbed in the human intestine (Yang et al., 2020). Temporal increases in the proportion of inorganic to total Hg has been shown in fish liver, suggesting active demethylation (Baatrup and Danscher, 1987; Cizdziel et al., 2003; Gonzalez et al., 2005). With MeHg generally considered to be more toxic than inorganic Hg, and acting partly on other cellular mechanisms, this illustrates a challenge in trying to characterize potential toxicity of Hg in wild-caught fish. In fish organs with low MeHg to total Hg ratio, the inorganic form can potentially contribute to the toxic response.

4.2. Differentially expressed genes in tusk with high Hg

In the present study, about 40% of the significant DEGs have previously been linked to Hg exposure (CTD, 2021). Differential expression of some of the genes in liver of the studied tusk could therefore partly be explained by other biological or chemical factors than Hg exposure. Se represents one potential confounding factor. Se levels, which can modify MeHg toxicity (Ralston and Raymond, 2010), did however not differ significantly between the four location or between the low and high Hg groups. In addition, field-collected fish will always contain a mixture of contaminants, of which many can affect transcription. Cd, which was higher in the high Hg group, had little effect on the gene lists and pathways according to the string pathway and network analyses (data not shown). The pathways enriched after controlling for Se, Cd and As levels were similar to those reported in Fig. 4 and in Supplementary file 5. The higher levels of organic pollutants and in particular PCB in liver of the high Hg tusk could possibly explain differing expression of AhR pathway-associated genes. Nevertheless, pathway analysis suggests that multiple molecular mechanisms of MeHg toxicity were affected in the high-Hg group. For example, neurotoxicity is one of the main effects of Hg in animals (Farina et al., 2011b). Differential expression of 130 out of 852 DEGs (15.2%) in the neurogenesis pathway in a non-neurological tissue such as liver is indicative of neurotoxic effects of MeHg. Furthermore, many of the significantly affected pathways are MeHg-sensitive according to exposure studies with fish under controlled laboratory settings (Ung et al., 2010; Richter et al., 2011; Yadetie et al., 2013, 2016; Tinant et al., 2021). We are therefore confident that the majority of the cause-effect relationships reported in this study are due to Hg exposure.

4.3. Protein stability and folding

Several DEGs encoding chaperones, a group of proteins that assist in protein folding and prevent non-specific aggregation, were differentially expressed in liver of tusk with high levels of Hg. Differential expression of chaperone DEGs could be an indication of Hg-induced endoplasmic reticulum (ER) stress in the cells. ER stress occurs when the burden of unfolded or misfolded protein in the

Table 3
Top Wikipathways based on 1230 differentially regulated genes (DEG).

Term	Overlap	P-value	Adjusted P-value	Odds Ratio	Combined Score	Genes
Notch Signaling Pathway WP61	12/61	0,00001	0,00223	4,56,430	52,80,949	PSENEN; NCOR2; NOTCH2; NUMBL; TLE1; NCOR1; NOTCH1; SNW1; MAML2; MAML1; EP300; PIK3R1
Androgen receptor signaling pathway WP138	15/90	0,00001	0,00307	3,86,698	46,18,371	SMARCE1; CREBBP; ROCK2; TGFB1I1; NCOA3; UBE3A; PIK3R1; NCOR2; KAT2B; AR; NCOR1; CREB1; ZNF318; EP300; CTNNB1
Nuclear Receptors WP170	9/38	0,00003	0,00409	5,49,518	58,01998	ESRRA; AR; THRB; NR5A2; VDR; HNF4A; RARB; PPARG; RXRG
Adipogenesis WP236	17/130	0,00004	0,00519	3,03409	30,43,901	STAT5B; GADD45A; CELF1; SERPINE1; LPL; IRS2; GATA4; KLF15; BMP4; NCOR2; KLF7; CREB1; NCOR1; CTNNB1; PPARG; LPIN1; RXRG
Heart Development WP1591	9/44	0,00009	0,00846	4,74,583	44,23,282	BMP4; BMPR2; NOTCH1; SRF; BHLHE40; CTNNB1; GATA4; NFATC1; VEGFA
Breast cancer pathway WP4262	18/154	0,00012	0,00924	2,71,191	24,54,082	NOTCH2; NOTCH1; GADD45A; FZD7; NCOA3; FZD9; LRP5; FZD8; PIK3R1; AXIN2; GADD45G; KIT; ERBB2; DVL2; CTNNB1; NBN; RAF1; FGFR1
VEGFA-VEGFR2 Signaling Pathway WP3888	23/236	0,00024	0,01589	2,26,120	18,88,764	HDAC4; ROCK2; SRF; CTNND1; PXN; GAB1; NFATC1; PIK3R1; EPN1; VEGFA; PPP3CA; GJA1; NR4A3; CREB1; CFL1; RAPGEF1; CTNNB1; MYH9; DNAJB9; FLNB; RAF1; PAK2; ATF4
miRNA regulation of prostate cancer signaling pathways WP3981	7/33	0,00043	0,02543	4,92,161	38,13,910	CASP9; AR; CREBBP; PLCL2; CTNNB1; IKBKG; RAF1
Aryl Hydrocarbon Receptor WP2586	8/46	0,00070	0,02546	4,03511	29,30,580	NCOR2; CDC37; CYP1A1; LPL; EP300; NCOA7; RAF1; VEGFA
Focal Adhesion-PI3K-Akt-mTOR-signaling pathway WP3932	26/303	0,00070	0,02742	1,99,092	14,47,103	PFKFB2; PFKFB1; PFKFB3; CAB39L; IRS2; PIK3R1; LAMC1; PIK3R5; HSP90B1; CASP9; ITGB7; IKBKG; EIF4B; ITGA3; LAMB2; VEGFA; COL1A1; KITLG; CREB1; CDC37; DDIT4; KIT; ITGA5; RAF1; ATF4; FGFR1
EGF/EGFR Signaling Pathway WP437	17/162	0,00064	0,02757	2,43,476	17,89,580	SH3GL3; USP8; STAT5B; NCOA3; GAB1; ASAP1; PIK3R1; EPN1; EPS8; GJA1; ATXN2; CREB1; CFL1; ERBB2; NCK2; RAF1; AP2M1
Notch Signaling WP268	8/45	0,00060	0,02840	4,12,477	30,58,851	NOTCH2; NCOR2; KAT2B; NUMBL; CREBBP; NOTCH1; MAML1; DVL2
PTF1A related regulatory pathway WP4147	4/11	0,00089	0,02990	8,43,704	59,29,510	KAT2B; NOTCH1; CTNNB1; PROX1
Focal Adhesion WP306	19/198	0,00096	0,03015	2,22,644	15,47,496	ITGA3; ROCK2; LAMB2; PXN; XIAP; ACTN4; PIK3R1; LAMC1; VEGFA; COL1A1; DIAPH1; ERBB2; RAPGEF1; CTNNB1; FLNB; ITGB7; ITGA5; RAF1; PAK2
Regulation of Wnt/B-catenin Signaling by Small Molecule Compounds WP3664	5/17	0,00059	0,03093	6,82,408	50,74,276	LRP1; FZD7; DVL2; FZD8; CTNNB1
Circadian rhythm related genes WP3594	19/201	0,00115	0,03381	2,19,321	14,85,104	TOP2A; DDX5; ZFHX3; ROCK2; SERPINE1; GFPT1; UBE3A; PROX1; TYMS; SLC6A4; F7; NCOR1; CREB1; MTA1; THRAP3; BHLHE40; EP300; PPARG; ATF4
Endometrial cancer WP4155	9/63	0,00144	0,03779	3,31,455	21,68,475	CASP9; GADD45A; ERBB2; CTNNB1; AXIN2; PIK3R1; RAF1; GADD45G; FGFR1
Epithelial to mesenchymal transition in colorectal cancer WP4239	16/159	0,00143	0,03971	2,33,478	15,29,253	NOTCH2; NOTCH1; FZD7; FZD9; LRP5; FZD8; PIK3R1; PROX1; TGFBR2; MAPK13; TJP1; ZEB2; LATS2; CTNNB1; ITGA5; RAF1
TGF-beta Receptor Signaling WP560	8/54	0,00207	0,04062	3,43,731	21,25,089	BMP4; ZEB2; CREBBP; SERPINE1; EP300; CTNNB1; SKIL; TGFBR2
Non-small cell lung cancer WP4255	9/66	0,00201	0,04124	3,16,389	19,64,687	CASP9; STAT5B; GADD45A; ERBB2; RARB; PIK3R1; RAF1; RXRG; GADD45G
Ethanol effects on histone modifications WP3996	6/31	0,00184	0,04134	4,49,068	28,28,375	HDAC4; KAT2B; ACSS2; MTHFR; ELP3; TYMS
Pathways Affected in Adenoid Cystic Carcinoma WP3651	9/65	0,00180	0,04256	3,21,256	20,29,743	KDM6B; SMARCE1; CREBBP; NCOR1; NOTCH1; NSD1; ERBB2; EP300; RAF1
Mesodermal Commitment Pathway WP2857	15/147	0,00173	0,04300	2,36,754	15,05566	MACF1; BMPR2; SRF; FZD8; AXIN2; EXT1; BMP4; EPB41L5; ARL4A; WDCP; HNF4A; BHLHE40; DNMT3B; RARB; FGFR1
Association Between Physico-Chemical Features and Toxicity Associated Pathways WP3680	9/66	0,00201	0,04312	3,16,389	19,64,687	DAAM1; ROCK2; FZD7; ERBB2; FZD9; FZD8; CTNNB1; RAF1; PFN2
Blood Clotting Cascade WP272	5/23	0,00259	0,04523	5,04388	30,04759	F7; SERPINE1; SERPINF2; KLKB1; F5
Prion disease pathway WP3995	6/33	0,00257	0,04669	4,21,852	25,15,579	SPI1; CREB1; EP300; NCAM1; HSP90B1; FGFR1
RAC1/PAK1/p38/MMP2 Pathway WP3303	9/68	0,00248	0,04681	3,07083	18,42,441	CASP9; STAT5B; PXN; ERBB2; CTNNB1; IKBKG; PIK3R1; ANGPTL1; MAPK13

lumen of ER changes. Numerous disturbances can induce ER stress, i.e., nutrient deprivation, lipid overload, infection, calcium and iron imbalance, hypoxia and oxidative stress. In addition, bio-accumulation of many xenobiotics, including toxic elements such as As, Pb, Cd and Hg, can trigger ER stress (Rana, 2020). For example, in a previous study with Atlantic salmon (*Salmo salar*) acutely exposed to metal-rich mine drainage water, pathway analysis predicted effects on protein processing in ER and steroid biosynthesis (Olsvik et al., 2016). Gene ontology analysis suggested that the treatment predominantly affected protein folding, possibly by disrupting disulfide bonds as a result of ER-generated stress. ER stress activated by intracellular signal transduction pathways is termed the unfolded protein response (Walter and Ron, 2013). The current dataset contained four DEGs associated with the unfolded protein response (*eif2ak4*, *atf4*, *hsp90b1* and *sec61g*). *Eif2ak4*, associated with autophagy and a paralog of *eif2ak3* (encodes PERK), and *atf4* were both higher expressed in liver tissue of tusk with high Hg accumulation. The signal transducer PERK controls one branch of the unfolded protein response by reducing the flux of protein to diminish ER stress (Walter and Ron, 2013). PERK activation typically leads to upregulation of ATF4, which in turn directs an antioxidant response that contributes to greater ER folding capacity (Adams et al., 2019). PERK-mediated induced translation of ATF4, a transcription factor that controls genes encoding components involved in apoptosis and autophagy, suggests elevated ER stress in cells with high concentrations of Hg. According to IPA upstream regulator analysis, 18 target molecules of the ATF4 transcription regulator were included in the dataset (*apba3*, *atf4*, *cdc42ep1*, *chac1*, *ctnnb1*, *ddit4*, *ddr2*, *gadd45a*, *hnf4a*, *hsp90b1*, *lars1*, *mrps7*, *nars1*, *pparg*, *slc1a5*, *slc7a3*, *vegfa*, *xpot*). Increased expression of ATF4 protein and mRNA has been shown in cells exposed to MeHg (Waldmann et al., 2017; Chung et al., 2019). However, since mobilization of PERK leads to phosphorylation of EIF2A and global downregulation of protein synthesis (Walter and Ron, 2013), the PERK-branch of the unfolded protein response and activated AFT4 cannot fully explain the increased expression of other transcripts in the unfolded protein pathway (e.g. *hsp70* (*hspa2* and *hspa8*) and *hsp40* (*dnajb1*) genes). Increased expression of these genes could

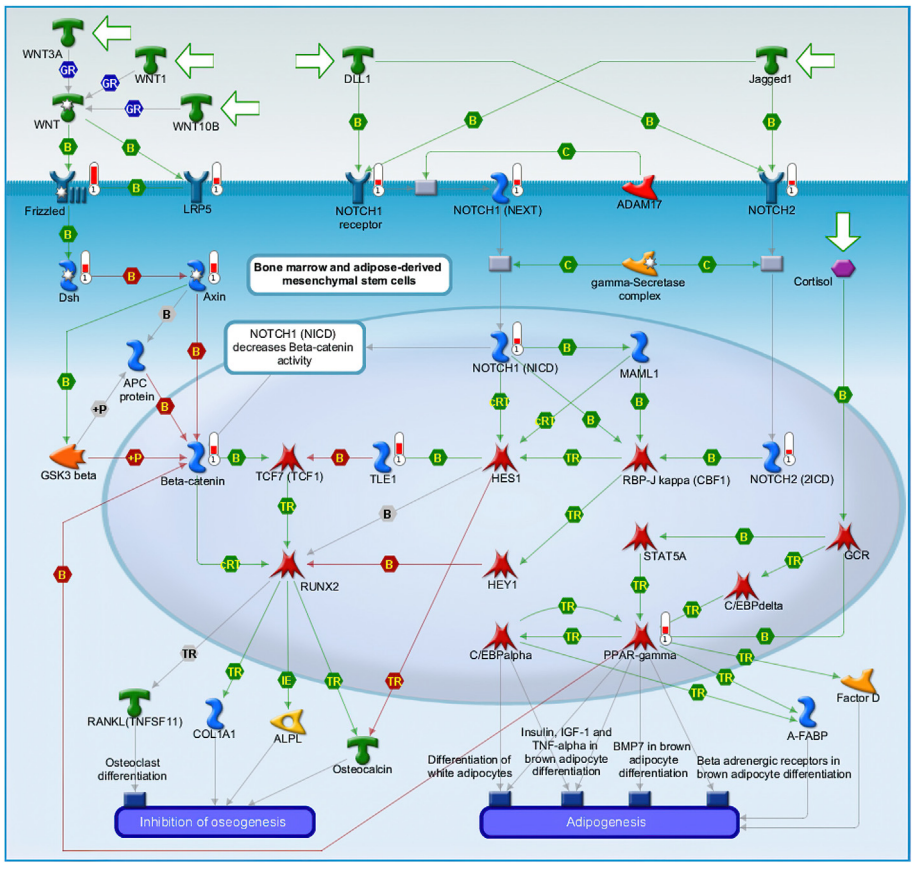

Fig. 6. Pathway map of the top significant Metacore Map in DEGs, *Stem cells_NOTCH in inhibition of WNT/Beta-catenin-induced osteogenesis* pathway, with interactions highlighted in the figure.

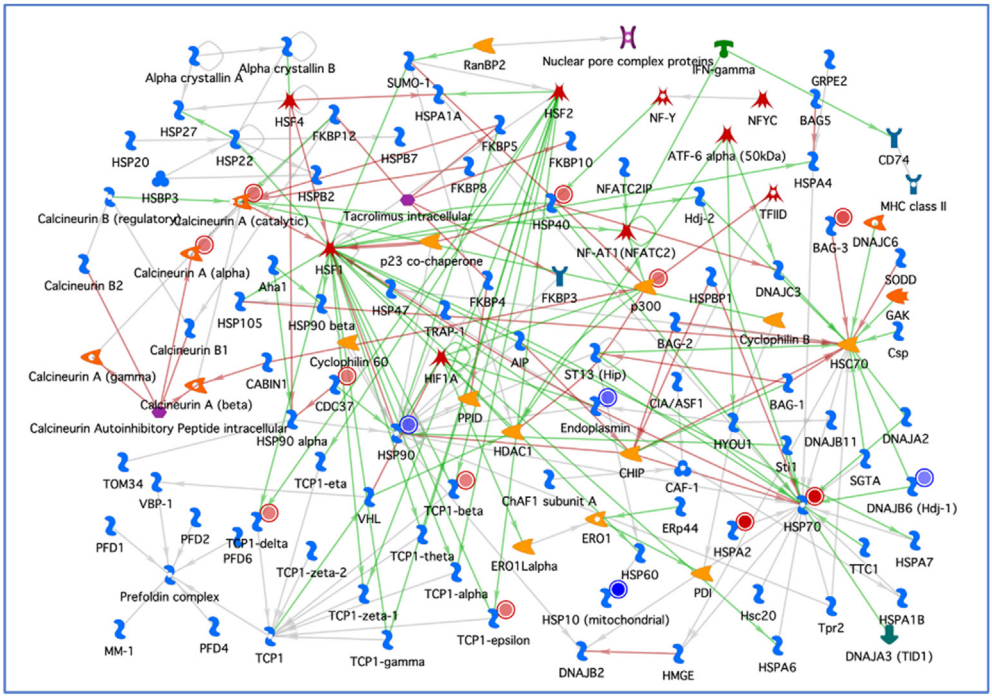

Fig. 7. Network for *protein folding: response to unfolded proteins*. This network is one of the significantly enriched MetaCore process networks (Supplementary file 3). Genes affected in high group Hg tusk are shown in red circles (upregulated) and blue (downregulated). Green, red and grey arrows indicate positive, negative and unspecified effects, respectively. (For interpretation of the references to color in this figure legend, the reader is referred to the Web version of this article.)

therefore rely on ER stress independent of the unfolded protein response. Terminally misfolded proteins can be degraded either through the ubiquitin–proteasome pathway or the lysosomal pathway (autophagy) (Bravo et al., 2013). It is therefore possible that the high levels of Hg have contributed to elevated degree of protein degradation in liver of the studied tusk.

In total, there were 26 DEGs associated with *cellular response to stress* (REACT:R-HSA-2262752). Interactions with Hg compounds have been shown for half of these before (inorganic Hg: *kdm6b*, *prkab1*, *psme2*, MeHg: *dnajb1*, *ep300*, *h1-0*, *map4k4*, *mdm4*, *nbn*, *tnik*, *vegfa*, both inorganic Hg and MeHg: *bag3*, *crebbp*) (CTD database). Interestingly, *crebbp* was the transcript that showed the second largest fold-change difference between the high and low-Hg groups. The protein encoded by *crebbp* has multiple functions, including activating transcription factor binding activity, and is a sensitive marker of oxidative stress (Dubreuil et al., 2020). We have previously shown that MeHg exposure increases *crebbp* transcription in liver of Atlantic cod (Yadetie et al., 2013). With differential expression of genes such as *gpx4* and *hmox1*, Hg-induced oxidative stress is a potential reason for the significant response seen on protein unfolding. In our previous study of tusk with elevated concentrations of Hg from Hardangerfjorden, RNA-seq analysis of a limited number of fish (3 fish with elevated Hg and 3 fish with lower levels) suggested Hg-induced hepatic effects on lipid metabolism and oxidative stress (Olsvik et al., 2013). The oxidative stress markers *gpx1* and *fth1* showed a correlation with accumulated levels of Hg. Furthermore, catalase activity was lower in tusk with high Hg concentrations. In addition, significantly lower levels of the antioxidant vitamin C were observed in liver of tusk with elevated concentrations of Hg (Olsvik et al., 2013). Oxidative stress, as shown by the activation of Nrf2 pathway and enriched network of response to unfolded proteins such as heat-shock proteins, was also one of the main affected pathways in liver of Atlantic cod exposed to 0.5 and 2.0 mg MeHg/kg, both at the transcriptional and protein levels (Yadetie et al., 2013, 2016). In our study here, three MetaCore process networks related to protein-folding (*Protein folding_Folding in normal condition*, *Protein folding_Protein folding nucleus* and *Protein folding_Response to unfolded proteins*) were enriched (Fig. 7, Supplementary file 3). Similarly, STRING networks identified significantly enriched GO BP terms related to protein-folding, such as *'de novo' protein folding*, *response to unfolded protein*, *protein stabilization* and *protein folding*, with in total 11 genes involved (Fig. 4, Supplementary file 5). The responses related to protein folding are highly similar to the transcriptome analysis in cod after a controlled laboratory exposure to MeHg, strongly suggesting that these effects can be ascribed to Hg toxicity. Two caspase DEGs, encoding protease enzymes playing essential roles in apoptosis, were differentially expressed in the present study. Differential expression of *casp1* (−2.4-fold) and *caps9* (2.10-fold) points to an imbalance of apoptosis mechanisms. In line with our findings, MeHg has been shown to activate the PERK/ATF4 branch of ER stress in mice kidney, followed by increased expression of CASP3 and CASP12 (Rojas-Franco et al., 2019). Similar findings have been reported in rat neurons, with MeHg-induced oxidative stress and apoptosis, and upregulation of ATF4 and CASP12 (Liu et al., 2019). *Ddit4*, which is regulated by ATF4 and encode a protein that regulates p53-mediated apoptosis in response to DNA damage, was 4.5-fold higher expressed in liver of the high-Hg tusk, further supporting a contaminant-induced effect on apoptosis. Taken together, oxidative stress and apoptosis may explain some of the observed transcriptional differences of DEGs associated with protein folding in liver of wild-caught tusk with low and high concentration of Hg.

4.4. Notch-signaling and adipogenesis

According to the Metacore and Enrichr analyses, mechanisms associated with Notch and Wnt signaling were differentially regulated in liver of tusk with high Hg. The Notch signaling pathway, the most significant pathway, is a highly conserved signaling system that regulates many aspects of development and tissue renewal. Misregulation of Notch signaling can lead to numerous disorders (Kopan and Ilagan, 2009). In humans, genome-scale sequencing studies have identified mutations in Notch genes in a broad spectrum of cancers (Aster et al., 2017). In *Drosophila*, MeHg as a neurotoxicant has been shown to induce Notch signaling (Bland and Rand, 2006; Prince and Rand, 2017). Exposure to other metals such as Cd can also activate Notch signaling, as shown in human renal proximal epithelial cells (Fujiki et al., 2014). In the present study, CTD enrichment analysis showed that 17 genes in the *signaling by Notch* pathway were differentially expressed in the high-Hg group, including the *notch1* and *notch2* receptors and *crebbp*. Of these, MeHg-gene/protein interactions have been shown for nine DEGs (*creb1*, *ep300*, *hdac4*, *kat2b*, *maml2*, *ncor2*, *notch1*, *tbl1xr1* and *tle1*), while *crebbp* is regulated by both inorganic Hg and MeHg (Ung et al., 2010; Yadetie et al., 2013). As the promoter of the *notch1* gene contains an antioxidant response element (ARE) and the Nrf2-ARE transcriptional machinery directly influence the magnitude of Notch signaling (Wakabayashi et al., 2015), Hg-induced oxidative stress may explain the observed effect on this pathway. Indeed, MeHg exposure is known to activate of NRF2 pathway, mediating antioxidant response (Ni et al., 2010).

Notch signaling has a role in adipocyte differentiation (adipogenesis), ranked as one of the most significant pathways differentially regulated in the high-Hg group. Adipocyte differentiation is regulated by a number of transcription factors, hormones and signaling pathways (Bi and Kuang, 2015). Differential regulation of adipogenesis was predicted based on 17 DEGs (*stat5b*, *gadd45a*, *celf1*, *serpine1*, *lpl*, *irs2*, *gata4*, *klf15*, *bmp4*, *ncor2*, *klf7*, *creb1*, *ncor1*, *ctnnb1*, *pparg*, *lpin1*, *rxrg*). *Pparg*, encoding a key regulator of adipocyte differentiation, was 2.3-fold higher expressed in liver of the high-Hg tusk. *Cebpb,* encoding another key regulator of adipogenesis (C/ERP), was one of the DEGs that separated the high-Hg group from the low-Hg group in the present examination using hierarchical clustering. Reassuringly, this result is in line with our previous study of tusk from Hardangerfjorden, where the hepatic transcriptional levels in fish with high Hg predicted effects on KEGG pathways adipocytokine signaling (ko04920) and PPAR signaling (ko03320) (two of the top three pathways) (Olsvik et al., 2013). Based on the DEGs associated with Notch signaling and adipogenesis in the present study, a possible outcome of Hg bioaccumulation in tusk liver might be disruption of mechanisms involved in fatty acid metabolism and osteogenesis.

4.5. Lipid metabolism

In liver, a possible outcome of activated adipogenesis could be lipid accumulation. Earlier studies have documented that *pparg* and other adipocyte-specific genes are expressed in hepatic steatosis (Gavrilova et al., 2003). Furthermore, liver-adipocyte crosstalk can contribute to lipid accumulation in the liver (Azzu et al., 2020). In support of this hypothesis, IPA pathway analysis predicted activated adipogenesis (based on 18 differentially regulated genes, of which 17 were higher expressed in the high Hg group), with hepatic steatosis as a significant pathway ($p = 3.87E-04$). Increased lipid accumulation has been observed in liver of zebrafish exposed to MeHg under controlled laboratory condition (Ung et al., 2010). Differential expression of a set genes associated with adipogenesis in liver of the studied tusk could therefore point to altered lipid

metabolism.

It is well established that Hg compounds can impact lipid metabolism in fish (Ung et al., 2010; Cambier et al., 2010; Richter et al., 2011), as well as in mammals (Ferrer et al., 2018). Sixty-three DEGs in the metabolism of lipids and lipoproteins pathway were differentially expressed in the high-Hg group in this study. Among them were three DEGs associated with PPAR signaling, *pparg*, *lpl* and *acsbg2*, all higher expressed in liver of the high-Hg tusk. In addition, four DEGs whose proteins are involved in β-oxidation were present in dataset, i.e. *acaa2*, *cetp*, *crot*, and *hadha*. PPARG controls fatty acid storage and glucose metabolism, suggesting an impact on energy metabolism. Up-regulation of many DEGs coding for fatty acid β-oxidation enzymes were also observed in liver of Atlantic cod exposed to MeHg for 14 days (Yadetie et al., 2013). Short-term exposure to $HgCl_2$ in zebrafish also induced effects on beta-oxidation (Ung et al., 2010). In a three-month feeding trial with Atlantic salmon, we found that 5 mg/kg MeHg affected hepatic transcription of *cpt1a* (Olsvik et al., 2011). The protein encoded by *cpt1a*, which was not differentially regulated in this study, is responsible for a rate limiting step in mitochondrial β-oxidation of fatty acids (Jogl et al., 2004). An impact on β-oxidation could be a result of Hg-induced accumulation of fat in the liver, as pathway analysis predicted an effect on the acetyl-L-carnitine metabolic network. One of the main functions of carnitine is the transfer of long-chained fatty acids to the mitochondria for subsequent β-oxidation (Longo et al., 2016). Hepatic steatosis, or accumulation of fat in the liver, is often observed in fish exposed to contaminants (Carnevali et al., 2017) and could be due to increased apoptosis or inflammation induced by oxidative stress. Mechanisms associated with β-oxidation therefore seem to be one of the targets of elevated Hg in tusk liver. Lipid metabolism is also known to be affected by persistent organic pollutants (Casals-Casas and Desvergne, 2011) and it is possible that these contaminants contributed to the observed responses in tusk liver.

In terms of predicted metabolic effect, two pathways associated with membrane lipids (phosphatidylcholine and phosphatidylinositol) were the most significant networks in the present study. Twenty-two DEGs associated with metabolism of phospholipids were differentially regulated in liver of tusk with high Hg concentration. These were *agpat5*, *cetp*, *cpne1*, *gpx4*, *lcat*, *lclat1*, *lipi*, *lpcat4*, *lpin1*, *lpl*, *mtmr1*, *mtmr14*, *pik3r1*, *pik3r5*, *pisd*, *pla2g12a*, *pla2g4c*, *pon1*, *ptpn13*, *scap*, *sptlc2*, and *stard10*. Interactions between MeHg and phospholipid membranes were described more than 20 years ago (Girault et al., 1997). In fathead minnow (*Pimephales promelas*), genes associated with phospholipid biosynthesis were affected by MeHg (Klaper et al., 2008). In rainbow trout, Ferain et al. (2018) showed that the phospholipid composition of liver cells impacts cell sensitivity to MeHg, whereas Tinant et al. (2021) showed that arachidonic acid (ARA, 20:4 n-6) was released in a dose-dependent manner in pre-adipocyte phospholipids after *in vitro* exposure to MeHg. In the latter study, impacts of MeHg exposure were also seen on eicosapentaenoic acid (EPA, 20:5 n-3) and docosahexaenoic acid (DHA, 22:6 n-3). For fish adapted to cold, deep-sea conditions, an Hg-induced imbalance in membrane phospholipid fatty acid profile (a shift in the PUFA n3/n-6 ratio) could potentially impact membrane fluidity and the well-being of the cells.

4.6. AhR pathway

Finally, it was interesting to note that the AhR pathway was differentially regulated in liver of tusk with high Hg levels. Pathway significance was based on the DEGs *ncor2*, *cdc37*, *cyp1a1*, *lpl*, *ep300*, *ncoa7*, *raf1*, and *vegfa*. In terms of the reactome pathway *cytochrome P450 - arranged by substrate type* that was enriched, there were five overlapping DEGs in the present dataset, *cyp1a1*, *cyp2r1*, *cyp3a5*, *nr1h4*, and *tbxas1*. With AhR as an upstream regulator, there were 30 target molecules in the dataset (shown in Table S6, Supplementary file 1). In mice it has been shown that Hg^{2+} potentiate the TCDD-induced effect on AhR-regulated genes (Korashy et al., 2005; Amara et al., 2012), but Hg compounds are generally not considered to be affecting the transcription of *cyp1a*. In this study, it is more likely that the observed effect on *cyp1a* and other AhR-regulated genes is caused by organic pollutants that were higher in tusk from the innermost part of the fjord. Deep-sea fish in western fjords of Norway not only contain high levels of Hg, but also tend to accumulate organic pollutants such as dioxins and dioxin-like PCBs, PCBs and PBDEs in fat-rich tissues (Frantzen and Maage, 2016). In addition, an aluminum plant in the innermost part of Sognefjorden (Hydro Aluminium AS in Årdal) represent a point source of PAHs (Kögel et al., 2017). Although the upstream regulator analysis did not predict significant AhR activation (AhR had an activation score of less than 2), it is likely that the differential expression of 30 target molecules of AhR rely on differential liver concentrations of organic pollutants such as dioxins, PCBs or PBDEs. However, the differentially regulated genes encoding solute carriers (24 DEGs in dataset) and ATP-powered pumps (3 DEGs in dataset) (shown in Table S7, Supplementary file 1) and transition metal homeostasis genes (Fig. 4), most strongly pointed to an impact on metal homeostasis. The three transporters with the largest fold change difference are all associated with metal ion transport. *Abcb6*, encoding a heavy metal importer, was 933-fold higher expressed in the high-Hg group, while *slc12a4*, encoding a potassium-chloride cotransporter, was 81-fold higher expressed in the high-Hg group. *Slc39a10*, encoding a Zn transporter, was 79-fold higher expressed in the high-Hg tusk. The copper-transporting ATPase 2 (*atp7b*) gene upregulated here was also upregulated by MeHg in Atlantic cod liver (Yadetie et al., 2013). Importantly, copper-transporting ATPase 2 has been shown to bind Hg, and it has the GMTCXXC motif conserved in binding domains of heavy metal transporters including bacterial Hg transporter proteins (DiDonato et al., 1997; Powlowski and Sahlman, 1999). The *slc47a2* (solute carrier family 47 member 2) gene that encodes a protein belonging to a family of transporters responsible for excretion of toxic cationic compounds was also upregulated. Its paralog *slc47a1* that has similar transporter function for cationic drugs was upregulated in MeHg treated cod liver (Yadetie et al., 2013), suggesting that *slc47a2* upregulation in tusk might be a response to MeHg exposure. By using the DEG list of 27 transporters as input in pathway analysis, Wikipathways Zn homeostasis (WP3529) and Nrf2 pathway (WP2884) scored highest. Taken together, and combined with the overall pathway analyses, the data strongly suggest a predominant effect of Hg exposure in the studied tusk. However, organic contaminants could be confounding factors in some of the responses. For example, some of the dioxin and dioxin-like-PCBs that activate the AHR pathway may also contribute some of the pathways enriched such as to oxidative stress (Reichard et al., 2006). The AHR pathway activation is likely a minor confounding effect since there was only a small (1.7-fold) higher average level (110.09 ng/g) of the dioxins and dioxin-like-PCBs in the high Hg group (Table 2). In contrast, much higher (10.6-fold) average Hg level (2.49 mg/kg) was detected in the high Hg group compared to the low Hg group (Table 2). Furthermore, controlling for the AHR ligand organic contaminant levels "sum dioxins and DL-PCBs" for a subset of samples resulted in largely similar results, with particularly similar pathways affected by Hg such as those related to responses to unfolded proteins (Fig. 4, Supplementary file 5, Supplementary file 6: Fig. S2A-C). Analysis controlling for "sum of PCB 7" (Supplementary file 6;

Fig. S3A and B) and PBDE7 (not shown) showed similar results with little effect on pathways related to Hg toxicity (Supplementary file 6: Fig. S3A and B), suggesting that controlling organic contaminants have little effect on the pathways enriched in the high Hg group, and particularly cellular processes related to protein folding show persistent enrichment. Thus, the predominant effects observed are likely caused by Hg contamination, although a certain level of confounding effects from other contaminants in the aquatic environment is expected.

In conclusion, this study documents Hg bioaccumulation in deep-water fish from fjords. Tusk caught in the innermost parts of Sognefjorden generally contained higher levels of Hg, but depth appears to be a confounding factor as fish caught at the greatest depth contained high concentrations of Hg. Molecular analysis predicts that accumulated Hg affects cellular mechanisms associated with protein stability and folding, adipogenesis, Notch signaling, and lipid metabolism in liver of the fish, all well-established markers of Hg toxicity. In terms of bioaccumulation and sublethal effects, this study shows that tusk from such fjords can be used to study Hg toxicity in wild populations of fish.

Credit author statement

PAO: Conceptualization, Funding acquisition, Methodology, Data curation, Writing- Original draft. AMA: Conceptualization, Field work, Methodology, Data curation, Reviewing and Editing. FY: Data curation, Visualization, Writing- Reviewing and Editing.

Declaration of competing interest

The authors declare that they have no known competing financial interests or personal relationships that could have appeared to influence the work reported in this paper.

Acknowledgment

The authors would like to thank the fishermen who helped collecting tusk and technical staff in the laboratories at the Institute of Marine Research (IMR) for help with sample preparation and chemical analyses. This study was supported by funding from IMR.

Appendix A. Supplementary data

Supplementary data to this article can be found online at https://doi.org/10.1016/j.chemosphere.2021.130588.

References

Adams, C.J., Kopp, M.C., Larburu, N., Nowak, P.R., Ali, M.M.U., 2019. Structure and molecular mechanism of ER stress signaling by the unfolded protein response signal activator IRE1. Front. Mol. Biosci. 6, 11.

Amara, I.E., Anwar-Mohamed, A., Abdelhamid, G., El-Kadi, A.O., 2012. Effect of mercury on aryl hydrocarbon receptor-regulated genes in the extrahepatic tissues of C57BL/6 mice. Food Chem. Toxicol. 50, 2325–2334.

Asplin, L., Johnsen, I.A., Sandvik, A.D., Albretsen, J., Sundfjord, V., Aure, J., Boxaspen, K.K., 2014. Dispersion of salmon lice in the Hardangerfjord. Mar. Biol. Res. 10, 216–225.

Aster, J.C., Pear, W.S., Blacklow, S.C., 2017. The varied roles of Notch in cancer. Annu. Rev. Pathol. 12, 245–275.

Azad, A.M., Frantzen, S., Bank, M.S., Nilsen, B.M., Duinker, A., Madsen, L., Maage, A., 2019a. Effects of geography and species variation on selenium and mercury molar ratios in Northeast Atlantic marine fish communities. Sci. Total Environ. 652, 1482–1496.

Azad, A.M., Frantzen, S., Bank, M.S., Johnsen, I.A., Tessier, E., Amouroux, D., Madsen, L., Maage, A., 2019b. Spatial distribution of mercury in seawater, sediment, and seafood from the Hardangerfjord ecosystem, Norway. Sci. Total Environ. 667, 622–637.

Azad, A.M., Frantzen, S., Bank, M.S., Madsen, L., Maage, A., 2020. Mercury bioaccumulation pathways in tusk (*Brosme brosme*) from Sognefjord, Norway: insights from C and N isotopes. Environ. Pollut. 269, 115997.

Azzu, V., Vacca, M., Virtue, S., Allison, M., Vidal-Puig, A., 2020. Adipose tissue-liver cross talk in the control of whole-body metabolism: implications in nonalcoholic fatty liver disease. Gastroenterology 158, 1899–1912.

Batchelar, K.L., Kidd, K.A., Drevnick, P.E., Munkittrick, K.R., Burgess, N.M., Roberts, A.P., Smith, J.D., 2013. Evidence of impaired health in yellow perch (*Perca flavescens*) from a biological mercury hotspot in northeastern north America. Environ. Toxicol. Chem. 32, 627–637.

Baatrup, E., Danscher, G., 1987. Cytochemical demonstration of mercury deposits in trout liver and kidney following methyl mercury intoxication: differentiation of two mercury pools by selenium. Ecotoxicol. Environ. Saf. 14, 129–141.

Berg, K., Puntervoll, P., Valdersnes, S., Goksøyr, A., 2010. Responses in the brain proteome of Atlantic cod (*Gadus morhua*) exposed to methylmercury. Aquat. Toxicol. 100, 51–65.

Bi, P., Kuang, S., 2015. Notch signaling as a novel regulator of metabolism. Trends Endocrinol. Metabol. 26, 248–255.

Bjornberg, K.A., Vahter, M., Grawe, K.P., Berglund, M., 2005. Methyl mercury exposure in Swedish women with high fish consumption. Sci. Total Environ. 341, 45–52.

Bland, C., Rand, M.D., 2006. Methylmercury induces activation of Notch signaling. Neurotoxicology (Little Rock) 27, 982–991.

Bloom, N.S., 1992. On the chemical form of mercury in edible fish and marine invertebrate tissue. Can. J. Fish. Aquat. Sci. 49, 1010–1017.

Blum, J.D., Popp, B.N., Drazen, J.C., Choy, C.A., Johnson, M.W., 2013. Methylmercury production below the mixed layer in the North Pacific Ocean. Nat. Geosci. 6, 879.

Bravo, R., Parra, V., Gatica, D., Rodriguez, A.E., Torrealba, N., Paredes, F., Wang, Z.V., Zorzano, A., Hill, J.A., Jaimovich, E., Quest, A.F., Lavandero, S., 2013. Endoplasmic reticulum and the unfolded protein response: dynamics and metabolic integration. Int. Rev. Cell Mol. Biol. 301, 215–290.

Bridges, C.C., Zalups, R.K., 2017. Mechanisms involved in the transport of mercuric ions in target tissues. Arch. Toxicol. 91, 63–81.

Cambier, S., Gonzalez, P., Durrieu, G., Maury-Brachet, R., Boudou, A., Bourdineaud, J.P., 2010. Serial analysis of gene expression in the skeletal muscles of zebrafish fed with a methylmercury-contaminated diet. Environ. Sci. Technol. 44, 469–475.

Carnevali, O., Notarstefano, V., Olivotto, I., Graziano, M., Gallo, P., Di Marco Pisciottano, I., Vaccari, L., Mandich, A., Giorgini, E., Maradonna, F., 2017. Dietary administration of EDC mixtures: a focus on fish lipid metabolism. Aquat. Toxicol. 185, 95–104.

Casals-Casas, C., Desvergne, B., 2011. Endocrine disruptors: from endocrine to metabolic disruption. Annu. Rev. Physiol. 73, 135–162.

Ceccatelli, S., Dare, E., Moors, M., 2010. Methylmercury-induced neurotoxicity and apoptosis. Chem. Biol. Interact. 188, 301–308.

Chapman, L., Chan, H.M., 2000. The influence of nutrition on methyl mercury intoxication. Environ. Health Perspect. 108, 29–56.

Chen, J., Bardes, E.E., Aronow, B.J., Jegga, A.G., 2009. ToppGene Suite for gene list enrichment analysis and candidate gene prioritization. Nucleic Acids Res. 37, W305–W311.

Chen, Y., Lun, A.T.L., Smyth, G.K., 2016. From reads to genes to pathways: differential expression analysis of RNA-Seq experiments using Rsubread and the edgeR quasi-likelihood pipeline. F1000Research 5, 1438.

Chung, Y.P., Yen, C.C., Tang, F.C., Lee, K.I., Liu, S.H., Wu, C.C., Hsieh, S.S., Su, C.C., Kuo, C.Y., Chen, Y.W., 2019. Methylmercury exposure induces ROS/Akt inactivation-triggered endoplasmic reticulum stress-regulated neuronal cell apoptosis. Toxicol 425, 152245.

Cizdziel, J., Hinners, T., Cross, C., Pollard, J., 2003. Distribution of mercury in the tissues of five species of freshwater fish from Lake Mead, USA. J. Environ. Monit. 5, 802–807.

Cole, D.C., Kearney, J., Sanin, L.H., Leblanc, A., Weber, J.P., 2004. Blood mercury levels among Ontario anglers and sport-fish eaters. Environ. Res. 95, 305–314.

CTD, 2021. The Comaprative Toxicogenomic Database [Data retrieved February. http://ctdbase.org.

Diez, S., 2009. Human health effects of methylmercury exposure. Rev. Environ. Contam. Toxicol. 198, 111–132.

DiDonato, M., Narindrasorasak, S., Forbes, J.R., Cox, D.W., Sarkar, B., 1997. Expression, purification, and metal binding properties of the N-terminal domain from the wilson disease putative copper-transporting ATPase (ATP7B). J. Biol. Chem. 26, 33279–33282.

Dubreuil, M.M., Morgens, D.W., Okumoto, K., Honsho, M., Contrepois, K., Lee-McMullen, B., Traber, G.M., Sood, R.S., Dixon, S.J., Snyder, M.P., Fujiki, Y., Bassik, M.C., 2020. Systematic identification of regulators of oxidative stress reveals non-canonical roles for peroxisomal import and the pentose phosphate pathway. Cell Rep. 30, 1417–1433 e1417.

EFSA, 2005. Opinion of the scientific panel on contaminants in the food chain on a request from the commission related to the presence of non dioxin-like polychlorinated biphenyls (PCB) in feed and food. EFSA J 284, 1–137.

EU, 2006. Commission Regulation (EC) No 1881/2006 of 19 December 2006 Setting Maximum Levels for Certain Contaminants in Foodstuffs (Including Various Subsequent Amendments). OJ L 364, 20.12.2006, pp. 5–24.

Farina, M., Aschner, M., Rocha, J.B., 2011a. Oxidative stress in MeHg-induced neurotoxicity. Toxicol. Appl. Pharmacol. 256, 405–417.

Farina, M., Rocha, J.B.T., Aschner, M., 2011b. Mechanisms of methylmercury-induced neurotoxicity: evidence from experimental studies. Life Sci. 89, 555–563.

Ferain, A., Bonnineau, C., Neefs, I., Das, K., Larondelle, Y., Rees, J.F., Debier, C., Lemaire, B., 2018. Transcriptional effects of phospholipid fatty acid profile on

rainbow trout liver cells exposed to methylmercury. Aquat. Toxicol. 199, 174–187.
Ferrer, B., Peres, T.V., Dos Santos, A.A., Bornhorst, J., Morcillo, P., Goncalves, C.L., Aschner, M., 2018. Methylmercury affects the expression of hypothalamic neuropeptides that control body weight in C57BL/6J mice. Toxicol. Sci. 163, 557–568.
Frantzen, S., Maage, A., 2016. Contaminants in wild-caught fish in coastal waters. Tusk, ling and other species.. NIFES report. In Norwegian with English summary.
Fujiki, K., Inamura, H., Matsuoka, M., 2014. Detrimental effects of Notch1 signaling activated by cadmium in renal proximal tubular epithelial cells. Cell Death Dis. 5, e1378.
Gavrilova, O., Haluzik, M., Matsusue, K., Cutson, J.J., Johnson, L., Dietz, K.R., Nicol, C.J., Vinson, C., Gonzalez, F.J., Reitman, M.L., 2003. Liver peroxisome proliferator-activated receptor gamma contributes to hepatic steatosis, triglyceride clearance, and regulation of body fat mass. J. Biol. Chem. 278, 34268–34276.
Grabherr, M.G., Haas, B.J., Yassour, M., Levin, J.Z., Thompson, D.A., Amit, I., Adiconis, X., Fan, L., Raychowdhury, R., Zeng, Q., Chen, Z., Mauceli, E., Hacohen, N., Gnirke, A., Rhind, N., di Palma, F., Birren, B.W., Nusbaum, C., Lindblad-Toh, K., Friedman, N., Regev, A., 2011. Full-length transcriptome assembly from RNA-Seq data without a reference genome. Nat. Biotechnol. 29, 644–652.
Girault, L., Boudou, A., Drfourc, E.J., 1997. Methyl mercury interactions with phospholipid membranes as reported by fluorescence, ^{31}P and ^{199}Hg NMR. Biochim. Biophys. Acta 1325, 250–262.
Gonzalez, P., Dominique, Y., Massabuau, J.C., Boudou, A., Bourdineaud, J.P., 2005. Comparative effects of dietary methylmercury on gene expression in liver, skeletal muscle, and brain of the zebrafish (*Danio rerio*). Environ. Sci. Technol. 39, 3972–3980.
Grieb, T.M., Driscoll, C.T., Gloss, S.P., Schofield, C.L., Bowie, G.L., Porcella, D.B., 1990. Factors affecting mercury accumulation in fish in the Upper Michigan Peninsula. Environ. Toxicol. Chem. 9, 919–930.
Jogl, G., Hsiao, Y.S., Tong, L., 2004. Structure and function of carnitine acyltransferases. Ann. N. Y. Acad. Sci. 1033, 17–29.
Julshamn, K., Frantzen, S., Valdersnes, S., Nilsen, B., Maage, A., Nederaas, K., 2011. Concentration of mercury, arsenic, cadmium and lead in fillets of Greenland halibut (*Reinhardtius hippoglossoides*) caught off the coast of northern Norway. Mar. Biol. Res. 7, 733–745.
Julshamn, K., Duinker, A., Berntssen, M., Nilsen, B.M., Frantzen, S., Nedreaas, K., Maage, A., 2013. A baseline study on levels of polychlorinated dibenzo-p-dioxins, polychlorinated dibenzofurans, non-ortho and mono-ortho PCBs, non-dioxin-like PCBs and polybrominated diphenyl ethers in Northeast Arctic cod (*Gadus morhua*) from different parts of the Barents Sea. Mar. Pollut. Bull. 75, 250–258.
Klaper, R., Carter, B.J., Richter, C.A., Drevnick, P.E., Sandheinrich, M.B., Tillitt, D.E., 2008. Use of a 15 k gene microarray to determine gene expression changes in response to acute and chronic methylmercury exposure in the fathead minnow *Pimephales promelas* Rafinesque. J. Fish. Biol. 72, 2207–2280.
Kögel, T., Frantzen, S., Azad, A.M., Maage, A., 2017. Seafood from Årdalsfjorden. Surveillance of polluted harbors and fjords 2016.. In: NIFES report. In Norwegian with English summary.
Kopan, R., Ilagan, M.X., 2009. The canonical Notch signaling pathway: unfolding the activation mechanism. Cell 137, 216–233.
Korashy, H.M., El-Kadi, A.O., 2005. Regulatory mechanisms modulating the expression of cytochrome P450 1A1 gene by heavy metals. Toxicol. Sci. 88, 39–51.
Kramer, A., Green, J., Pollard Jr., J., Tugendreich, S., 2014. Causal analysis approaches in ingenuity pathway analysis. Bioinformatics 30, 523–530.
Kuleshov, M.V., Jones, M.R., Rouillard, A.D., Fernandez, N.F., Duan, Q., Wang, Z., Koplev, S., Jenkins, S.L., Jagodnik, K.M., Lachmann, A., McDermott, M.G., Monteiro, C.D., Gundersen, G.W., Ma'ayan, A., 2016. Enrichr: a comprehensive gene set enrichment analysis web server 2016 update. Nucleic Acids Res. 44, W90–W97.
Kvangarsnes, K., Frantzen, S., Julshamn, K., Sæthre, L.J., Nedreaas, K., Maage, A., 2012. Distribution of mercury in a gadoid fish species, tusk (*Brosme brosme*), and its implication for food safety. J. Food Sci. Eng. 2, 603–615.
Lamborg, C.H., Hammerschmidt, C.R., Bowman, K.L., Swarr, G.J., Munson, K.M., Ohnemus, D.C., Lam, P.J., Heimburger, L.E., Rijkenberg, M.J., Saito, M.A., 2014. A global ocean inventory of anthropogenic mercury based on water column measurements. Nature 512, 65–68.
Longo, N., Frigeni, M., Pasquali, M., 2016. Carnitine transport and fatty acid oxidation. Biochim. Biophys. Acta 1863, 2422–2435.
Liu, W., Yang, T., Xu, Z., Xu, B., Deng, Y., 2019. Methyl-mercury induces apoptosis through ROS-mediated endoplasmic reticulum stress and mitochondrial apoptosis pathways activation in rat cortical neurons. Free Radic. Res. 53, 26–44.
Lundebye, A.K., Lock, E.J., Rasinger, J.D., Nostbakken, O.J., Hannisdal, R., Karlsbakk, E., Wennevik, V., Madhun, A.S., Madsen, L., Graff, I.E., Ornsrud, R., 2017. Lower levels of persistent organic pollutants, metals and the marine omega 3-fatty acid DHA in farmed compared to wild Atlantic salmon (*Salmo salar*). Environ. Res. 155, 49–59.
Maage, A., Bjelland, O., Olsvik, P., Nilsen, B., Julshamn, K., 2012. Contaminants in fish and seafood products 2011: Mercury in deep-water fish and shellfish from Hardangerfjorden and in marine oils. NIFES report. In Norwegian with English summary.
Morel, F.M.M., Kraepiel, A.M.L., Amyot, M., 1998. The chemical cycle and bioaccumulation of mercury. Annu. Rev. Ecol. Systemat. 29, 543–566.
Ni, M., Li, X., Yin, Z., Jiang, H., Sidoryk-Wegrzynowicz, M., Milatovic, D., Cai, J., Aschner, M., 2010. Methylmercury induces acute oxidative stress, altering Nrf2 protein level in primary microglial cells. Toxicol. Sci. 116, 590–603.
Olsvik, P.A., Amlund, H., Torstensen, B.E., 2011. Dietary lipids modulate methylmercury toxicity in Atlantic salmon. Food Chem. Toxicol. 49, 3258–3271.
Olsvik, P.A., Lindgren, M., Maage, A., 2013. Mercury contamination in deep-water fish: transcriptional responses in tusk (*Brosme brosme*) from a fjord gradient. Aquat. Toxicol. 144–145, 172–185.
Olsvik, P.A., Amlund, H., Saele, O., Ellingsen, S., Skjaerven, K.H., 2015. Impact of dietary selenium on methylmercury toxicity in juvenile Atlantic cod: a transcriptional survey. Chemosphere 120, 199–205.
Olsvik, P.A., Ulvund, J.B., Teien, H.C., Urke, H.A., Lie, K.K., Kristensen, T., 2016. Transcriptional effects of metal-rich acid drainage water from the abandoned Lokken Mine on Atlantic salmon (*Salmo salar*) smolt. J. Toxicol. Environ. Health A 79, 612–632.
Powlowski, J., Sahlman, L., 1999. Reactivity of the two essential cysteine residues of the periplasmic mercuric ion-binding protein. MerP. J. Biol. Chem. 274, 33320–33326.
Prince, L.M., Rand, M.D., 2017. Notch target gene E(spl)mdelta is a mediator of methylmercury-induced myotoxicity in Drosophila. Front. Genet. 8, 233.
Ralston, N.V., Raymond, L.J., 2010. Dietary selenium's protective effects against methylmercury toxicity. Toxicology 278, 112–123.
Rana, S.V.S., 2020. Endoplasmic reticulum stress induced by toxic elements-a review of recent developments. Biol. Trace Elem. Res. 196, 10–19.
Reichard, J.F., Dalton, T.P., Shertzer, H.G., Puga, A., 2006. Induction of oxidative stress responses by dioxin and other ligands of the aryl hydrocarbon receptor. Dose Response 3, 306–333.
Richter, C.A., Garcia-Reyero, N., Martyniuk, C., Knoebl, I., Pope, M., Wright-Osment, M.K., Denslow, N.D., Tillitt, D.E., 2011. Gene expression changes in female zebrafish (*Danio rerio*) brain in response to acute exposure to methylmercury. Environ. Toxicol. Chem. 30, 301–308.
Rojas-Franco, P., Franco-Colin, M., Torres-Manzo, A.P., Blas-Valdivia, V., Thompson-Bonilla, M.D.R., Kandir, S., Cano-Europa, E., 2019. Endoplasmic reticulum stress participates in the pathophysiology of mercury-caused acute kidney injury. Ren. Fail. 41, 1001–1010.
Rua-Ibarz, A., Bolea-Fernandez, E., Maage, A., Frantzen, S., Sanden, M., Vanhaecke, F., 2019. Tracing mercury pollution along the Norwegian Coast via elemental, speciation, and isotopic analysis of liver and muscle tissue of deep-water marine fish (*Brosme brosme*). Environ. Sci. Technol. 53, 1776–1785.
Tinant, G., Neefs, I., Das, K., Rees, J.-F., Larondelle, Y., Debier, C., 2021. Methylmercury displays pro-adipogenic properties in rainbow trout preadipocytes. Chemosphere 263, 127917.
Ung, C.Y., Lam, S.H., Hlaing, M.M., Winata, C.L., Korzh, S., Mathavan, S., Gong, Z., 2010. Mercury-induced hepatotoxicity in zebrafish: in vivo mechanistic insights from transcriptome analysis, phenotype anchoring and targeted gene expression validation. BMC Genom. 11, 212.
Valdersnes, S., Maage, A., Fliegel, D., Julshamn, K., 2012. A method for the routine determination of methylmercury in marine tissue by GC isotope dilution-ICP-MS. J. AOAC Int. 95, 1189–1194.
Van den Berg, M., Birnbaum, L.S., Denison, M., De Vito, M., Farland, W., Feeley, M., Fiedler, H., Hakansson, H., Hanberg, A., Haws, L., Rose, M., Safe, S., Schrenk, D., Tohyama, C., Tritscher, A., Tuomisto, J., Tysklind, M., Walker, N., Peterson, R.E., 2006. The 2005 World Health Organization reevaluation of human and Mammalian toxic equivalency factors for dioxins and dioxin-like compounds. Toxicol. Sci. 93, 223–241.
Wakabayashi, N., Chartoumpekis, D.V., Kensler, T.W., 2015. Crosstalk between Nrf2 and notch signaling. Free Radic. Biol. Med. 88, 158–167.
Waldmann, T., Grinberg, M., Konig, A., Rempel, E., Schildknecht, S., Henry, M., Holzer, A.K., Dreser, N., Shinde, V., Sachinidis, A., Rahnenfuhrer, J., Hengstler, J.G., Leist, M., 2017. Stem cell transcriptome responses and corresponding biomarkers that indicate the transition from adaptive responses to cytotoxicity. Chem. Res. Toxicol. 30, 905–922.
Walter, P., Ron, D., 2011. The unfolded protein response: from stress pathway to homeostatic regulation. Science 334, 1081–1086.
Wang, K., Munson, K.M., Beaupre-Laperriere, A., Mucci, A., Macdonald, R., Wang, F.Y., 2018. Subsurface seawater methylmercury maximum explains biotic mercury concentrations in the Canadian Arctic. Sci. Rep-Uk 8, 14465.
Wiener, J.G., Krabbenhoft, D.P., Heinz, G.H., Scheuhammer, A.M., 2003. Ecotoxicology of mercury. In: Hoffman, D.J., Rattner, B.A., Burton, G.A., Cairns, J. (Eds.), Handbook of Ecotoxicology. Lewis Publishers, Boca Raton, FL, pp. 409–463.
Yadetie, F., Karlsen, O.A., Lanzen, A., Berg, K., Olsvik, P., Hogstrand, C., Goksoyr, A., 2013. Global transcriptome analysis of Atlantic cod (*Gadus morhua*) liver after in vivo methylmercury exposure suggests effects on energy metabolism pathways. Aquat. Toxicol. 126, 314–325.
Yadetie, F., Bjorneklett, S., Garberg, H.K., Oveland, E., Berven, F., Goksoyr, A., Karlsen, O.A., 2016. Quantitative analyses of the hepatic proteome of methylmercury-exposed Atlantic cod (*Gadus morhua*) suggest oxidative stress-mediated effects on cellular energy metabolism. BMC Genom. 17, 554.
Yang, L., Zhang, Y., Wang, F., Luo, Z., Guo, S., Strahle, U., 2020. Toxicity of mercury: molecular evidence. Chemosphere 245, 125586.
Zhou, Y., Zhou, B., Pache, L., Chang, M., Khodabakhshi, A.H., Tanaseichuk, O., Benner, C., Chanda, S.K., 2019. Metascape provides a biologist-oriented resource for the analysis of systems-level datasets. Nat. Commun. 10, 1523.